creative commons

COMMONS DEED

저작자표시-비영리-변경금지 2.0 대한민국

이용자는 아래의 조건을 따르는 경우에 한하여 자유롭게

- 이 저작물을 복제, 배포, 전송, 전시, 공연 및 방송할 수 있습니다.

다음과 같은 조건을 따라야 합니다:

저작자표시. 귀하는 원저작자를 표시하여야 합니다.

비영리. 귀하는 이 저작물을 영리 목적으로 이용할 수 없습니다.

변경금지. 귀하는 이 저작물을 개작, 변형 또는 가공할 수 없습니다.

- 귀하는, 이 저작물의 재이용이나 배포의 경우, 이 저작물에 적용된 이용허락조건을 명확하게 나타내어야 합니다.
- 저작권자로부터 별도의 허가를 받으면 이러한 조건들은 적용되지 않습니다.

저작권법에 따른 이용자의 권리는 위의 내용에 의하여 영향을 받지 않습니다.

이것은 이용허락규약(Legal Code)을 이해하기 쉽게 요약한 것입니다.

Disclaimer

dCollection

공학박사학위논문

타이어 노면 마찰 추정 및 센서 불확실성을 활용한 강건한 자동비상제동알고리즘 개발

Robust Autonomous Emergency Braking Algorithm using the Tire-road Friction Estimation and the Sensor Uncertainties

2015 년 2 월

서울대학교 대학원

기계항공공학부

이 태 영

타이어 노면 마찰 추정 및 센서 불확실성을 활용한 강건한 자동비상제동알고리즘 개발

Robust Autonomous Emergency Braking Algorithm using the Tire-road Friction Estimation and the Sensor Uncertainties

지도교수 이 경 수

이 논문을 공학박사 학위논문으로 제출함

2015년 2월

서울대학교 대학원
기계항공공학부
이 태 영

이태영의 공학박사 학위논문을 인준함

2015년 2월

위 원 장 : 고 상 근 (인)
부위원장 : 이 경 수 (인)
위 원 : 차 석 원 (인)
위 원 : 송 한 호 (인)
위 원 : 강 연 식 (인)

Abstract

Robust Autonomous Emergency Braking Algorithm using the Tire-road Friction Estimation and the Sensor Uncertainties

Taeyoung Lee
School of Mechanical and Aerospace Engineering
The Graduate School
Seoul National University

Safe and collision-free travel is vital in today's society. It is also an important issue in many industrial processes. Therefore the automakers are trying to help drivers to avoid or mitigate collision with active safety systems instead of passive safety systems. For example, ACC (Adaptive Cruise Control) and AEBS (Advanced Emergency Braking System) warn the driver from rear-end collision risk and intervene by partial braking maneuvers have already been implemented in modern passenger vehicles in recent years.

Since the active safety system always work with a human driver co-existing, the longitudinal safety system must be acceptable to the driver. Thus the system operation law need to be set based on the human driver's driving characteristics. In order to be acceptable to drivers, vehicle behavior or driving characteristics of the control in target situation needs to be similar to the human drivers. Therefore, in this thesis, the longitudinal safety control algorithm was not only designed by using the physical collision risk but also by driver's characteristic to achieve 'safe and acceptable' control algorithm.

In the case of road information, previous research about friction estimation was used to estimate the tire-road friction information. To make up for

unreliability in normal steady driving situation, some assumptions were applied in the case of normal steady-straight driving condition. By using the estimated tire-road friction information, safety indices for the control mode decision were redefined.

Generally, measured sensor signal has difference with true value due to the measurement noise or uncertainty. To guarantee the robust control performance, RADAR and vision sensor are used. For robust control mode decision, the simple static theory and Kalman filter considering the measurement noise are used in this research. The expected error range of the longitudinal safety index from the measurement noise can be defined from the covariance matrix of the Kalman filter and simple definition of the deviation of the function. By using the expected error, the threshold of new longitudinal safety index was determined for the safety monitoring of the driving situation.

The proposed vehicle longitudinal safety algorithm was evaluated through computer simulations using vehicle simulation software, CARSIM and MATLAB/Simulink in two kinds of scenario: 1) emergency braking in steady following driving, 2) stop preceding vehicle in the rainy day situation. Also, to confirm the robustness of the proposed control algorithm, the simulation was conducted 100 iteration in the same scenario. From simulation results, it can be concluded that the proposed longitudinal safety algorithm could enhanced the longitudinal safety and guarantee the robust capacity from the sensor uncertainty and various road condition.

Keywords: Advanced Emergency Braking System, Sensor uncertainty, Tire-road friction coefficient, Longitudinal Safety Control, Collision Avoidance

Student Number: 2007-22993

Contents

Abstract i

List of Tables v

List of Figures vii

Chapter 1 Introduction 1

1.1 Background and Motivation 1

1.2 Previous Researches..... 7

1.3 Thesis Objectives 9

1.4 Thesis Outline 11

Chapter 2 Advanced Emergency Brake Algorithm..... 12

2.1 Safety Index for Longitudinal Safety Assessment 13

2.2 New Safety Index for Longitudinal Safety Control 26

2.3 Safety Threshold for the New Longitudinal Safety Index ... 29

Chapter 3 Sensor Information Analysis and Environment Information based Longitudinal Safety Control Algorithm... 39

3.1 Environment Information for Vehicle Longitudinal Safety Control 40

3.2 Tire-road fricition Estimation 46
3.3 Safety Monitoring by using the Environment information.. 50
3.4 Sensor Information for
Vehicle Longitudinal Safety Control 56
3.5 Sensor Data Fusion 67
3.6 Control Mode Decion by using the Fused Sensor Data..... 76

Chapter 4 Simulation of the Vehicle Longitudinal 81
4.1 Simulation with/without fused sensor information
for longitudinal safety algorithm 83
4.2 Simulation with tire-road friction information
for longitudinal safety algorithm 91

Chapter 5 Conclusions 98

Bibliography 101

국문초록 108

List of Tables

Table 2.1 Definition of the relation between SV and PV 15
Table 2.2 Required signals for calculating each safety index 20
Table 2.3 Warning index and TTC for various ranges of deceleration 23
Table 2.4 Control Threshold values of the TTC for the AEB algorithm 36
Table 2.5 Linear coefficient of the Time gap in Car following situation ...38
Table 2.6 Control Threshold values of the Warning Index for the AEB algorithm 38

Table 3.1 Longitudinal stiffness change with various conditions 44
Table 3.2 LPTB and LPTS for partial braking and emergency braking situation 53
Table.3.3 Initial Setting Condition for Sensor data collection 59
Table 3.4 Variance and Standard deviation value of range error: RADAR sensor 62
Table 3.5 Variance and Standard deviation value of range error: Vision sensor 63
Table 3.6 Standard deviation value of range error 63
Table 3.7 Variance and Standard deviation value of range rate error: RADAR sensor 65
Table 3.8 Variance and Standard deviation value of range rate error: Vision sensor 66
Table 3.9 Standard deviation value of range error 66
Table 3.10 Standard deviation value and propagation gain for estimated clearance 72
Table 3.11 Standard deviation value and propagation gain for estimated relative velocity 73

Table 4.1 Results of 100 simulation
with/without fused sensor information 89
Table 4.2 Results of 100 simulation
with/without tire-road friction information 97

List of Figures

Figure 1.1 Road fatalities and road vehicles in Germany along with the introduction of ADAS from 1953 to 2012 3

Figure 1.2 Causalities by environmental condition 5

Figure 2.1 Control Flow of the AEB algorithm.....12

Figure 2.2 Relation between SV and PV 14

Figure 2.3 The looming effect 16

Figure 2.4 Test vehicle for logging manual-driving data 22

Figure 2.5 Analysis of the indexes for various rates of deceleration 24

Figure 2.6 Trajectory of the warning index and the inverse TTC for deceleration 25

Figure 2.7. New safety index in TTC-Warning index plane.....27

Figure 2.8. Collision risk level of the new safety index in TTC-Warning index plane.....28

Figure 2.9 Driver's Steering Characteristics under Different Speed 30

Figure 2.10 Driver's Steering Characteristics under Different Driving Situations 31

Figure 2.11. Longitudinal Acceleration – Velocity Relation 34

Figure 2.12 Threshold values of the TTC in normal braking for the AEB algorithm 35

Figure 3.1 Friction coefficient On Wet Asphalt 42

Figure 3.2 Friction coefficient on dry asphalt 43

Figure 3.5 Tire information estimation architecture 46

Figure 3.6 Structure of the tire force estimator 47

Figure 3.7 Tire-road friction coefficient estimator scheme 48

Figure 3.8 Braking distance by tire-road friction 51
Figure 3.9 Distance of the LPTS by tire-road friction 53
Figure 3.10 Threshold for Emergency Braking by tire-road friction 54
Figure 3.11 Test Vehicle for sensor system 59
Figure 3.12. Range Error vs. Range 60
Figure 3. 13 Range data of RADAR sensor and Vision sensor 61
Figure 3.14 Range Error vs. Range : RADAR sensor 62
Figure 3.15 Range Error vs. Range: Vision sensor 63
Figure 3.16. Range rate Error vs. Range rate 64
Figure 3. 17 Range rate data of RADAR sensor and Vision sensor 64
Figure 3.18 Range rate Error vs. relative velocity: RADAR sensor 65
Figure 3.19 Range rate Error vs. relative velocity: Vision sensor 66
Figure 3.20. Assumption of the sensor data fusion 68
Figure.3.21 variance of the measured clearance data 71
Figure.3.22 Weighting Factor and Sensor Detection Range 71
Figure.3.23 variance of the measured relative velocity data 73
Figure 3.24 Scheme of a Kalman Filter 75
Figure 3.25 Expected error of the Longitudinal Safety Index 79
Figure 3.26 Expected error of the Longitudinal Safety Index 80

Figure 4.1 Simulation scenario to evaluate the performance of enhanced longitudinal safety: with/without fused sensor information ..83
Figure 4.2 Simulation results: with/without fused sensor information ...86
Figure 4.3 Simulation results: with/without fused sensor information ...88
Figure 4.4 Simulation results from 100 iterations: with/without fused sensor information 89
Figure 4.5 Figure 4.5 Simulation scenario to evaluate the performance of enhanced longitudinal safety: with/without tire-road friction information 92

Figure 4.6 Simulation results:
with/without tire-road friction information 94
Figure 4.7 Simulation results:
with/without tire-road friction information 96
Figure 4.8 Simulation results from 100 iterations:
with/without tire-road friction information 97

Chapter 1

Introduction

1.1 Background and Motivation

The National Policy statistics in Korea reported that the total number of deaths in 2010 caused by traffic accidents in Korea is 5,505, about 2.6 per 10,000 cars and twice the OECD average of 1.3[Choi 13]. In the case of Korea, there is the unenviable record being one of the highest traffic accidents and fatality rates. In 2009, there were 5,838 fatalities on the road. One of the important accident type is related with longitudinal collision in various scenarios. The longitudinal collision is investigated to the most frequent type of crash from Traffic Accident Analysis Center's report [Road Traffic Accidents in Korea 2009].

Passive safety systems, such as seat belts, airbags or active head-rest, etc., are already part of almost each vehicle. Therefore, advanced driver assistance systems (ADAS) or active safety systems are supposed to be able to significantly contribute to reduce the number of road fatalities.

Therefore the automakers are trying to help drivers to avoid or mitigate collision with active safety systems instead of passive safety systems. Practical applications have become possible due to significant progress in sensors, actuators, and other enabling technologies. Several systems already commercialized include Adaptive Cruise Control (ACC), Traffic Jam Assist (TJA), Lane Keeping Support (LKS), Lane Change Assist (LCA), Blind Spot Detection (BSD), Automated Parking Assist (APA) and Forward Collision Warning System (FCWS) [Minoiu09, An06, Moon09, Seiler98, Vahidi03, Rimini05].

Especially, ACC and FCWS warn the driver from rear-end collision risk and intervene by partial braking maneuvers when an accident is imminent have already been implemented in modern passenger vehicles in recent years.

As statistics in [Bundesamt13] show that more than 60% of all road accidents in Germany are caused by collisions between vehicles, collision warning (CW), collision mitigation (CM) and even collision avoidance (CA) systems are currently focused to improve road safety.

According to the 7th General plan for Transportation Safety which has been enforced since 2012, the establishment of strategies to make full use of active safety system is the key project to reduce road casualty by 3,000 (40% 0f 2010's level) to achieve middle level ranking among OECD countries by 2016. In particular, under the umbrella of the United Nations Economic Commission for Europe (UN/ECE), at the World Forum for Harmonization of Vehicle Regulations (WP29), the 2002 ITS Informal Group was created to review standards associated with the safety of vehicles, passengers and related active

safety system[Choi 13].

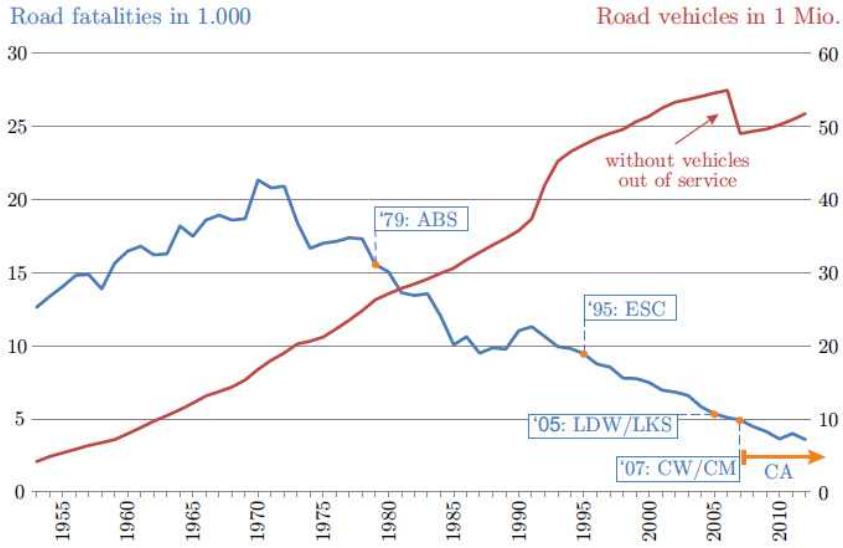

Figure 1.1 Road fatalities and road vehicles in Germany along with the introduction of ADAS from 1953 to 2012(derived from [Bundesamt13])

As a results, Euro NCAP has released its updated rating scheme for 2013-2016 that outlines, amongst other technologies, the implementation of Autonomous Emergency Braking (AEB) technologies within the overall rating scheme. Three types of AEB technologies will be included in the rating scheme, starting with low speed car-to-car AEB City and higher speed car-to-car AEB Inter-Urban in 2014, followed two years later by AEB Pedestrian [R. Schram 13] .

Since the active safety system always work with a human driver co-existing, the longitudinal safety system must be acceptable to the driver and the system's operation law need to set based on the human driver's driving characteristics.

In order to be acceptable to drivers, vehicle behavior or driving characteristics of the control in target situation need to be similar to the human drivers.

This is based on the assumption that, if the controlled vehicle behavior is set based on the vehicle behavior of ‘experienced average drivers’ manual driving, then the longitudinal safety controller may be considered as a ‘reference-driver’ for the human driver in longitudinal driving motion. The reference-driver is an attentive driver who conducts vehicle longitudinal control actions to provide the driver with safe driving in rear-end collision possible driving situations and to keep safe vehicle-to-vehicle clearance in severe braking situations although driver didn’t concentrate or recognize driving situation. The concept of the ‘reference-driver’ is the motivation of the analysis and investigation of manual driving data and the safety indices for the design of the longitudinal safety control algorithm proposed.

Moreover, these systems operated usually based on the assumption that RADAR or vision sensor data is actual values of driving situation which measured the clearance and the relative velocity with noise and uncertainty. Also, road condition is assumed as dry-asphalt condition which is not guaranteed in real driving condition. Major drawbacks resulting from this basic approach cannot perform adequate reactions in various road condition.

The Casualties by environment condition are summarized as shown in Figure 1.2. The 8% of crash is related with bad climate condition such as rain, cloudy, fog or snow which cause sensing error or unexpected braking capacity of the control system [Road Traffic Accidents in Korea 2012].

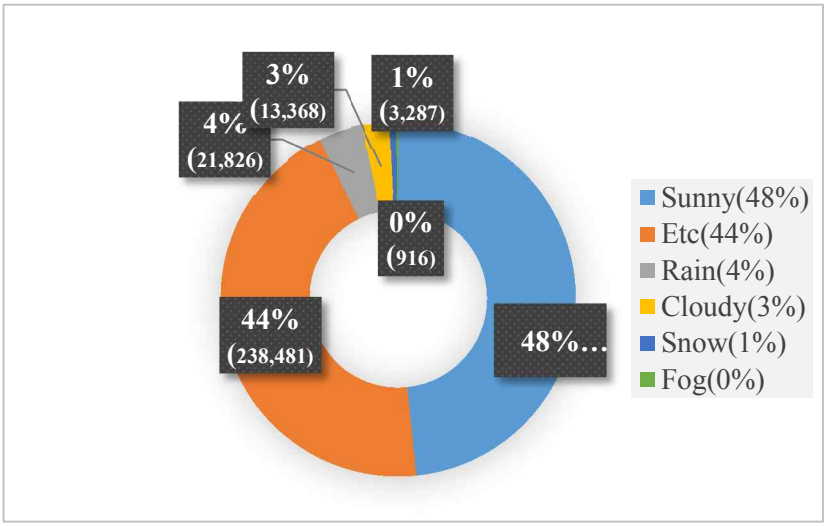

Figure 1.2 Causalities by environmental condition

Tire-road friction influences the ability of tires to generate steering, traction, and braking forces and thus affects vehicle motion. Knowledge of the friction coefficient of the road is thus important for the design and analysis of vehicle control systems, especially active safety systems. In order to maintain longitudinal safety capacity, it is imperative that the braking capabilities of subject vehicle in the system be conservatively estimated. Also, it is also necessary that be estimated its influences as closely as possible to its actual environmental condition.

In order for the longitudinal safety system to provide a positive and beneficial influence towards the reduction of potential crashes, it is critical that the safety system has the ability to correctly identify the vehicle, pedestrian and object targets in the vehicle's path [Zhang 06]. Environmental sensors have a limited field of view and uncertainty or error terms this usually leads to unexpected

control failure or poor control performance.

The solution to this problem relies primarily on the longitudinal safety system's sensing system ability to estimate the detection range, relative speed, etc. between the subject vehicle and all other appropriate targets.

This dissertation describes a vehicle longitudinal safety control algorithm by using the analysis of environment information and sensor information. In order to develop acceptable and safe longitudinal control system, not only road information and sensor information analysis, but also the driving characteristic based safety indices analysis is conducted.

1.2 Previous Researches

Various longitudinal safety control algorithms have been studied previously by many researchers. Combined throttle/brake control for vehicle longitudinal control with applications to vehicle platoon control and autonomous intelligent vehicles has been investigated by several researchers since 1970's [Shladover, Chien 94, St. Germann 95,]. Vehicle-to-vehicle distance control algorithm studies, control system implementation and development of ACC and Stop-and-Go have been conducted in 1990's. In past decades, Human-driver driving behavior has been analyzed in various scenarios. Human driver driving behavior has been studied by several researchers. The contribution of the cognitive approach is the formation of a driver's knowledge database and the modeling of the cognitive processes underlying the driving activity. Also, several researchers have focused their research on manual driving behavior and its application to the human-centered design of ACC and/or CW/CA systems. A longitudinal driver model that was developed on the basis of measured driving data and the evaluation of the impact of ACC vehicles on traffic flow was presented by Peng [H. Peng 02]. Drivers' crash-avoidance behavior and the effect of ABS on drivers' ability to avoid a collision in a crash-imminent situation were reported by Larson [Larson 05].

For the automatic brake control, the risk of collision is estimated. The time-to-collision (TTC) is a time distance between preceding and subject vehicle [Fancher00]. It uses relative velocity and clearance which can be easily

obtained signal from front RADAR. However the TTC is not designed to consider speed of subject vehicle and acceleration of subject and preceding vehicle. Therefore several indices are proposed for longitudinal collision risk estimation. The warning index is designed to represent a maximum braking distance [Moon08]. Differently with TTC, it can consider the speed of subject vehicle. The perceptual risk estimate (PRE), modified TTC or several indices are also proposed to consider the speed of subject vehicle, acceleration of subject and preceding vehicle [Aoki11, Kusano11, Jansson08, Yeo11].

Ferrara and Vecchio [Ferrara 08] designed a second-order sliding mode control system based on a nonlinear vehicle model. Zhu and Feng [Zhu 12] presented a single neuron PID tracking control strategy for overtaking behavior. Nouveli`ere and Mammar [Nouveli`ere 07] proposed an experimental implementation of a shared vehicle longitudinal controller based on a second-order sliding mode technique, which was tested under usual traffic conditions such as stop-and-go, stopping at obstacles, and car-following in a number of scenarios, but it mainly concentrated on the low velocity.

Although many research results on CW/CA systems have been published, there are no full collision avoidance systems that function at high speed fitted to production vehicles at present. Besides, most of the forward collision warning and collision mitigation braking systems currently fitted to production vehicles mainly only function in specific condition.

1.3 Thesis Objectives

This dissertation propose longitudinal safety algorithm to prevent or mitigate the rear-end collision by braking maneuver. Since the proposed safety system work with a human driver together, the longitudinal safety system must be acceptable to the driver. The key is to ensure that control signals are given at the appropriate time. In order to make proper control system, characteristics of existing safety indices were discussed through a theoretical comparison. Then the longitudinal safety control algorithm was designed by using not only the physical collision risk but also driver's characteristic to achieve 'safe and acceptable' control algorithm.

Tire-road friction influences the ability of tires to generate steering, traction, and braking forces and thus affects vehicle motion. Knowledge of the friction coefficient of the road is thus important for the design and analysis of vehicle control systems, especially active safety systems. However, in many researches on the collision avoidance system, road condition had been assumed in specific condition such as dry asphalt situation. In order to maintain longitudinal safety capacity, previous research about friction estimation was used to estimate the tire-road friction information. To make up for unreliability in normal steady driving situation, some assumption was applied in the case of normal steady-straight driving condition. By using the estimated tire-road friction information, safety indices for the control mode decision were redefined to detect the reliable collision risk monitoring in the non-dry asphalt driving situation.

The clearance and the relative velocity is essential signals for safety

monitoring in the longitudinal safety control. However, these measured sensor signals include a measurement noise or uncertainty. These difference values of the measurement signal influence to the safety indices for safety monitoring. Therefore, the sensor information analysis and fused measurement signals are used to design the safety monitoring and control mode decision. For robust control mode decision, the simple static theory and Kalman filter is used in this research. The expected error range of safety indices from the measurement noise can be defined from the covariance matrix of the Kalman filter and simple definition of the deviation of the function. By using the expected error, the threshold of each safety index was determined for the safety monitoring of the driving situation.

The performance of the proposed algorithm has been evaluated via analysis of simulation using vehicle simulation software, CARSIM and MATLAB/Simulink.

1.4 Thesis Outline

This dissertation can be divided into the following three parts.

The first part deals with an automated collision avoidance algorithm using safety indices. To develop the new longitudinal safety index, characteristics of existing safety indices were discussed through a theoretical comparison. Also, threshold values of safety indices were determined based on the physical collision risk and driver's characteristic. The control mode determines warning level and braking level to maintain the longitudinal safety by using safety indices and threshold values.

The vehicle longitudinal safety control algorithm for collision avoidance using environment information and a sensor information have been proposed in the second part of the dissertation. For robust control mode decision, the simple static theory and Kalman filter by using the measurement noise is used in this research. Also, friction estimated module was used to environment information estimation. By using the fused obstacle information and tire-road friction information, safety monitoring and control mode decision was determined.

At the final parts, the simulation results in order to evaluate the proposed control algorithm. Also, to confirm the robustness of the proposed control algorithm, the simulation was performed 100 iteration in the same scenario.

The conclusions are presented after the final parts.

Chapter 2

Advanced Emergency Braking Algorithm

In order to develop the acceptable and efficient longitudinal safety system, it is important to select appropriate safety indices and apply them to longitudinal safety system. Therefore, characteristics of existing safety indices were discussed through a theoretical comparison. As a results, new longitudinal safety index was designed by using the 'TTC' and 'Warning Index' for driving safety monitoring.

The overall control flow is shown in Figure.2.1

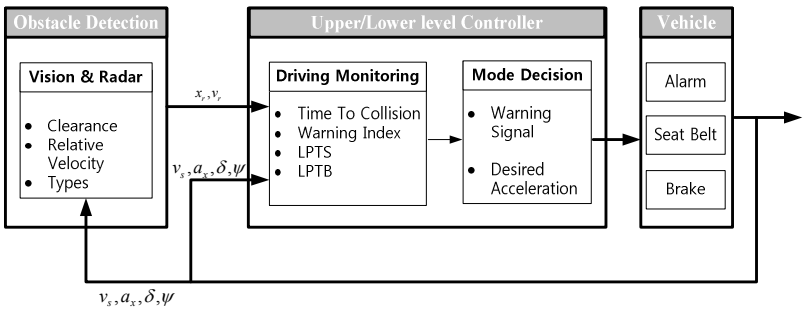

Figure 2.1 Control Flow of the AEB algorithm

2.1. Safety Indices for Longitudinal Safety Assessment

A considerable amount of research has been performed on collision waning systems, which are the first step to assist drivers in collision avoidance. In the view point of preventive safety, deceleration assistance control is effective when collision risk is high and it is difficult for the driver to avoid it. On the other hand, driver can feel anxiety or nuisance against the system if the initiation timing of automatic brake and/or deceleration profile is not appropriate and it may make the system inefficient. The key is to ensure that control signals are given at the appropriate time, i.e., just in time for drivers to react and avoid collisions while not too early or too frequent to become a nuisance distraction to drivers.

In the prior work, several measures were defined to characterize the emergency level of various dynamic situations, and different sets of human-vehicle experiments were carried out to calibrate these measures to human performances and reactions, based on which different warning criteria were developed to assist drivers [Lee 11]. However, there was no single index good enough to estimate the risk of a rear-end collision because there are various types of traffic situations in the real world. Furthermore, no clear guideline has been established for selecting a suitable index for a given situation.

Thus, in order to develop the acceptable and efficient longitudinal safety system, it is important to select appropriate safety indices and apply them to longitudinal safety system.

This study categorizes the established safety indices as Time relative Indices and Braking relative Indices. Time relative indices are selected the following three indices for discussion – 'Time Headway(THW)', 'Time To Collision(TTC)' and '2nd order Time To Collision'. In the case of braking relative indices, 'Margine To Collision(MTC)' and 'Warning Index(X)' are selected.

2.1.1. Definition of Variable for Safety Indices

As shown in Figure 2.2, the variables for safety indices can be defined. Interaction between the subject vehicle (SV) and the preceding vehicle (PV) is analyzed utilizing variables. The variables can be categorized the one's motion and relative movement of each vehicle. Relative position is defined as positive when SV is behind PV. In the case of the relative velocity (v_{rel}), positive value is defined when v_s is higher than v_p.

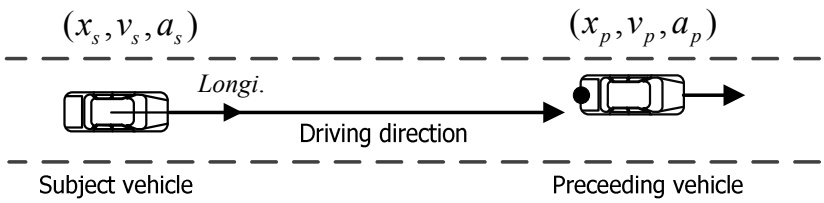

Figure 2.2 Relation between SV and PV

2.1.2. Time Relative Indices

Time relative indices are mainly concerned about driver's awareness of the danger. Although, many kinds of the indices are used to evaluate the system performance, in this research two indices are selected for discussion – 'Time To Collision(TTC)' and 'Time Headway(THW)'.

Table 2.1 Definition of the relation between SV and PV

Category		Definition
Position	Subject Vehicle	x_s
	Preceding Vehicle	x_p
	Relative	$x_r = c = x_p - x_s$
Velocity	Subject Vehicle	v_s
	Preceding Vehicle	v_p
	Relative	$v_{rel} = v_s - v_p$
Acceleration	Subject Vehicle	a_s
	Preceding Vehicle	a_p

A. Time Headway (THW)

'Time-Headway(THW)' is most commonly measured as the distance from the tip of one vehicle to the tip of the next one behind it, expressed as the time it will take for the trailing vehicle to cover that distance. THW is defined by dividing c by v_s. Therefore THW can be regarded as a margin depending on the velocity of SV.

$$THW = \frac{c}{v_s} \tag{2.1}$$

In steady following situations, a driver's awareness of risk is determined only

by THW [Kondo 06].Time headway is important because it specifies how much time the following driver has to react in case the lead vehicle suddenly brakes at maximum deceleration level.

B. Time To Collision (TTC)

'Time to Collision (TTC)' is defined as the time left to a collision between SV and PV assuming that the current relative velocity remains constant.

The TTC, which is a well-known parameter in longitudinal safety systems, is defined as from the definition of the TTC:

$$TTC = \frac{c}{v_r} \tag{2.2}$$

The TTC is related to the visual cues that might guide driver headway maintenance. The concept of looming, as described in human-factor studies, is employed in the analysis of human perception and longitudinal control behavior in driving situations. The looming effect was first investigated by Hoffman and Mortimer (1996) and was a key factor in the human-centered design of an ACC-with-braking and forward-crash-warning system undertaken by Fancher et al. [Fancher 00]. As illustrated in Figure 2.3, the size of the image that is projected onto the eye of the following driver depends on the range of the observed object, i.e., the preceding vehicle. If there is relative motion between the vehicles, the range, R, and the angle, θ, will change.

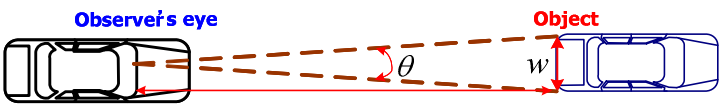

Figure 2.3 The looming effect

The width of the preceding vehicle, w, is constant and can be represented as

$$w = R \cdot \theta \qquad (2.3)$$

The rate of change of the range is related to the rate of change of the angle, θ, which is occluded by the image as projected onto the observer's eye, i.e., the driver's eye, as follows:

$$\frac{dw}{dt} = 0 = \dot{R} \cdot \theta + R \cdot \dot{\theta} \qquad (2.4)$$

The looming effect is represented by the ratio of the occluded angle to the rate of change of that angle, i.e. $\theta / \dot{\theta}$. Therefore, the looming effect can be represented as:

$$\frac{\theta}{\dot{\theta}} = \frac{R}{-\dot{R}} = \frac{c+l}{v_{rel}} \approx TTC \qquad (2.5)$$

In Eq. (2.5), l is the distance between the front bumper and the driver's eye. As shown in Eq. (2.5), the driver's sensation of looming is related to the TTC, which is computed using the range and the rate of change of the range.

C. 2nd order TTC (TTC^{2nd})

The second-order-predicted TTC (TTC2nd) denotes the estimated time to collision assuming that the current relative acceleration is maintained.

$$TTC^{2nd} = \frac{v_{rel} + \sqrt{{v_{rel}}^2 - 2 \cdot a_r \cdot c}}{a_r} \qquad (2.6)$$

The value of the original TTC is not exactly the same as the actual remaining time when either SV or PV changes its velocity. In contrast, TTC^{2nd} is more

accurate than TTC when the relative acceleration rate between SV and PV is non-zero and constant such as just after driver brake operation [Barber, P].

2.1.3. Braking Relative Indices

For discussion, Margine to Collision and Warning Index are selected as braking relative indices. Braking relative indices are driven by using vehicle's physical braking movement.

A. Margine to Collision (MTC)

The 'Margin to Collision (MTC)' is dimensionless index which evaluates the final position of FV and PV when the two vehicles are supposed to slow down simultaneously with maximum deceleration. [Kondo 06]

$$MTC = \frac{-c + d_p}{d_s} = \frac{-c - \dfrac{v_p^{\,2}}{2 \cdot a_p}}{-\dfrac{v_s^{\,2}}{2 \cdot a_s}} \qquad (2.7)$$

MTC evaluates the risk in proportion to the square of velocity by considering the braking distance of both vehicles. If MTC is less than one, because it is difficult for a driver to avoid a collision, the collision risk is high. MTC assumes abrupt deceleration to evaluate the potential risk by using the each vehicle's acceleration. This information can reflect the appropriateness of driver braking based on the relationship of velocity changes between the two vehicles.

B. Warning Index (x)

The non-dimensional warning index represents the danger of physical collision in the current driving situation and is defined as follows [Yi 99]:

$$x = \frac{c - d_{br}}{d_w - d_{br}} \tag{2.8}$$

The warning-critical and braking-critical distances are defined as follows:

$$\begin{aligned} d_{br} &= v_{rel} \cdot t_{brake} - \frac{v_{rel}^{\ 2}}{2a_{x,\max}} \\ d_w &= v_{rel} \cdot t_{thinking} + v_{rel} \cdot t_{brake} - \frac{v_{rel}^{\ 2}}{2a_{x,\max}} \end{aligned} \tag{2.9}$$

where, t_{brake} is the system delay, which is given by the brake-system hardware, $a_{\max}$ is the maximum deceleration of the vehicle under driving conditions, $t_{thinking}$ is the delay in human response between recognition and manipulation [Cho 10].

These terms can be derived from the kinematics of the two vehicles that brake to a full stop. If the vehicles start at this distance and brake with their maximum decelerations, they will come to a stop with their bumpers touching each other. To make the critical distance more conservative, two delay terms are added; these account for system and driver delays.

If range exceeds d_{br} and d_w, then the warning index is a positive value that is greater than unity and indicates that the current driving situation is in a safe region. If range is below d_{br}, then the warning index is a negative value and indicates that the current driving situation can be dangerous.

From Equation (2.8) and (2.9), it is shown that the warning index can be influenced by using the maximum deceleration which was able to be obtained

from the friction estimation methods.

2.1.4. Safety Indices for Longitudinal Safety Control

Five safety indices indicate longitudinal collision risk level based on relative movement of SV and PV. Here we discuss the relationships among these five indices. To appropriately analyze the rear-end collision risk, it is important to select an evaluation index based on these characteristics.

Table 2.2 Required signals for calculating each safety index

Safety Index	**Required Signals**				
	c	v_s	v_p	a_s	a_p
THW	○	○			
TTC	○	○	○		
TTC^{2nd}	○	○	○	▼	▼
MTC	○	○	○	○	□
x **(Warning Index)**	○	○	○	▼	▼

○: measurable **▼: assumption** **□:Required but Unmeasurable**

As demonstrated in Eq. (2.1), THW is defined by dividing c (which reflects relative movement of both vehicles) by vs. Therefore, THW can be regarded as a margin depending on the velocity of SV. According to the definition of the THW, abrupt deceleration or acceleration situation is not suitable situation for using the THW to evaluate the safety.

TTC is derived assuming that the current relative velocity remains constant.

However, it is not practical to use between the same velocity PV and SV. For example, if the velocity of the PV and SV is same, although the clearance is very short, there is no way to check the estimation of the driver's risk awareness caused by the closeness between PV and SV. However, TTC is related with 'Looming effect' which is a well-known physical quantity that a driver is able to obtain from visual information. Therefore, it may be appropriate for longitudinal safety control system to consider as a driver's sense of the collision risk level.

TTC^{2nd} is the quadratic value of TTC and indicates the correct time to collide with PV when the relative acceleration between FV and PV is non-zero and constant. However, to calculate TTC2nd, it is necessary to obtain acceleration, which is very noisy and unmeasurable in detection sensors(RADAR or Vision sensor).

MTC is indicating the margin to collision with PV, not for regulating the driver's braking. MTC indicates the margin by representing the degree based on criterion utilizing the braking distance of SV. MTC assumes the abrupt deceleration of both PV and FV. As well as, as indicated in Table 2.2, MTC is calculated utilizing the relative acceleration.

The warning index represents the danger of physical collision in the current driving situation based on warning-critical and braking-critical distances. Because warning index assumes maximum deceleration of both SV and PV as same level, it can be judged driving condition as excessive dangerous situation.

In longitudinal safety systems such as Adaptive Cruise Control (ACC) system or Collision Warning/Collision Avoidance (CW/CA) system, TTC is well-

known parameters. As discussed, TTC is suitable for assessments of safety measure with the vehicle in front of the speed difference between the vehicle and its leader is maintained. On the other hand, 'Warning Index' is physically driven index based on the driving situation and considered as maximum deceleration of the vehicle.

Figure 2.4 Test vehicle for logging manual-driving data.

To compare the tendency of the warning index and the TTC in various longitudinal driving condition, Field Operational Test data(FOT data) acquation was conduct. The FOT data was collected using a test vehicle equipped with various sensors, e.g., a laser RADAR, a CCD camera, a three axis inertial sensor, a brake pedal force sensor, a steering angle sensor, a yaw rate sensor, a data logging computer, and a GPS. Manual-driving data were collected in a highway, a perimeter road, and urban area. The velocity varies between 0(km/h) and 120(km/h). To make up for the FOT data's diversity, the FOT database, which is collected by KATECH (Korea Automotive Technology Institute), was

added to analysis.

In this context, relationships between the warning index and the deceleration of the subject vehicle have been investigated using manual-driving data. The mean and percentile values of the warning index and the TTC are computed for ranges of deceleration. Comparisons of the warning index and the TTC for four ranges of deceleration are given in Tables 2.3, respectively.

Table 2.3 Warning index and TTC for various ranges of deceleration

Acceleration/Mean	Warning Index	TTC
$-2 < a < -0.5$ m/s^2	1.41	9.10
$-4 < a < -2$ m/s^2	0.98	4.00
$-6 < a < -4$ m/s^2	0.82	1.43
$a < -6$ m/s^2	0.13	0.89

As illustrated in Table 2.3, the magnitude of the warning index and the TTC significantly decreases as the vehicle's deceleration increases. This implies that the driver's perception, decision, and manipulation cause large deceleration as the warning index and the TTC decreases. Therefore, the warning index and the TTC can be used to determine a driving situation.

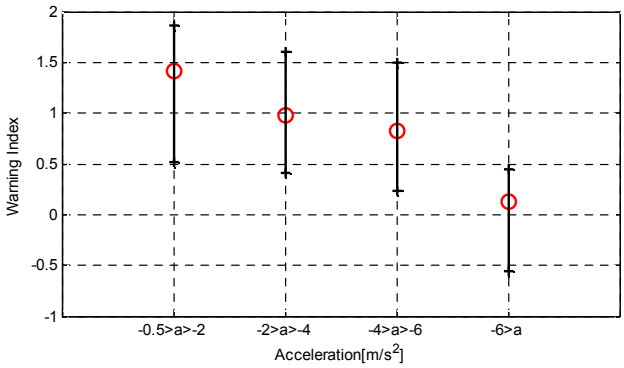

(a) Warning index

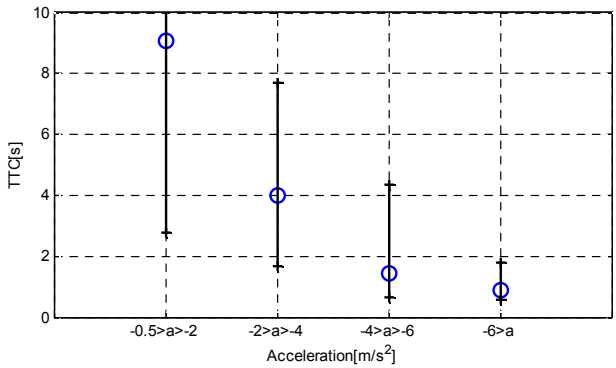

(b) TTC

Figure 2.5 Analysis of the indexes for various rates of deceleration

As shown in Figure 2.6, the driving situations can be analyzed in a two-dimensional graph of the warning index vs. the TTC. When the warning index and the TTC is high, the driving situation is in a safe region. However, if the warning index and the TTC gradually decreases, the danger of a rear-end collision increases and the vehicle needs to decelerate to avoid the warning region. When the warning index and the TTC is low, the driving situation is critical and therefore, the emergency brake should be applied.

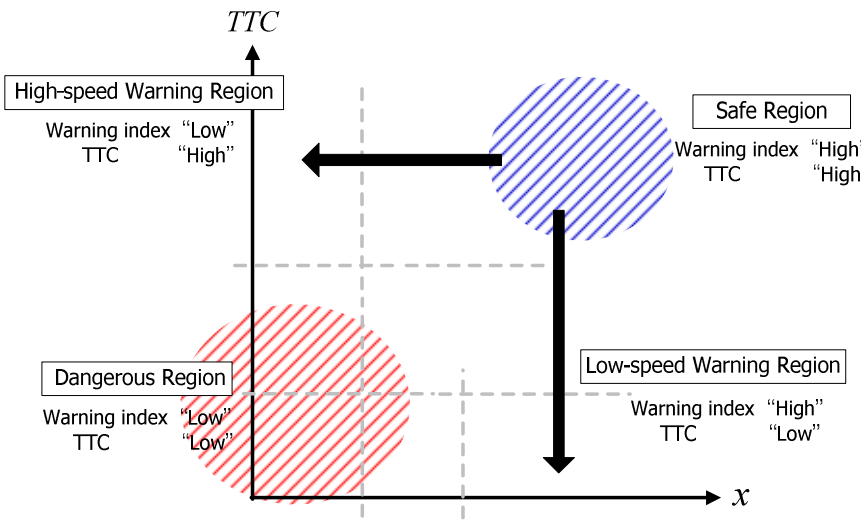

Figure 2.6 Trajectory of the warning index and the inverse TTC for deceleration

2.2 New Safety Index for Longitudinal Safety Control

The new safety index that can indicate the danger of longitudinal collision now can be introduced. The SLongi is defined by using 'Warning Index' and 'TTC'. In order to determine the safety index, a safety threshold and significant factors with respect to each index should be determined.

Collision risk can be indicated as a radius of the collision risk circle from the partial threshold point (normal braking threshold) to present state. Significant factors which can determine the S_{Longi} are classified into three categories: 1) present states of the vehicle, 2) threshold value in the Maginot line of the normal driving and 3) threshold value of the emergency situation. Using the description of the present states and threshold values above, the new longitudinal safety index can be defined as:

$$S_{Longi} = \sqrt{\left(\frac{TTC - TTC_{Partial}}{TTC_{Emergency} - TTC_{Partial}}\right)^2 + \left(\frac{x - x_{Partial}}{x_{Emergency} - x_{Partial}}\right)^2} \qquad (2.10)$$

To normalize the collision risk between TTC and Warning index, a denominator for the each normalized safety index was constructed as difference between emergency threshold and partial threshold value of each safety index. A numerator was defined as distance from present safety level and the partial threshold values in normalized safety index plane.

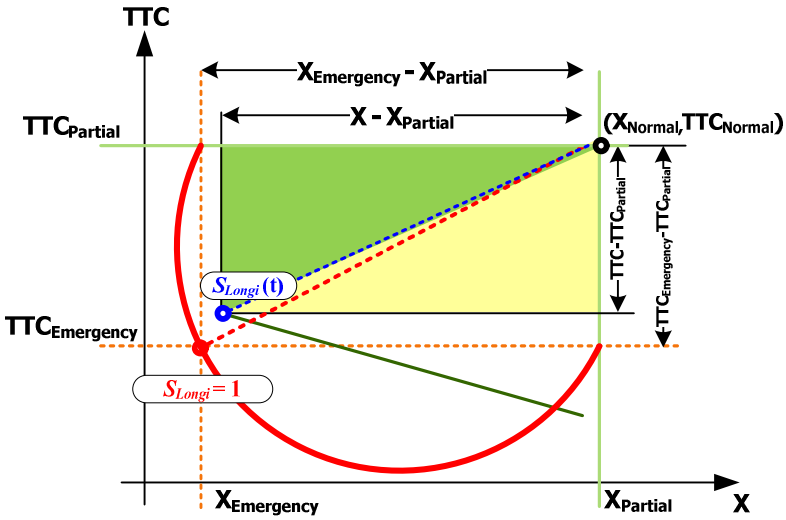

(a) Safety index relation in TTC-Warning Index plane

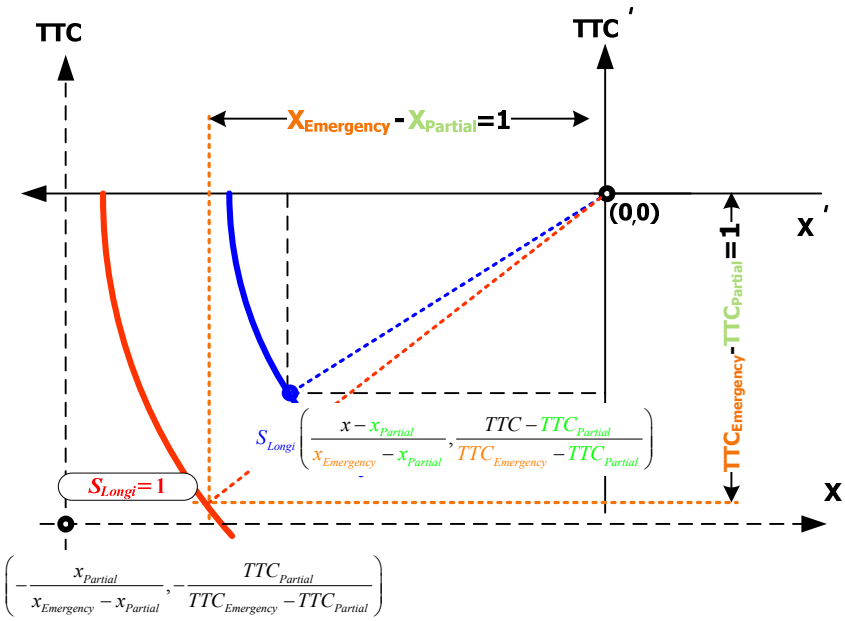

(b) New safety index calculation in Normalized TTC-Warning Index plane

Figure 2.7. New safety index in TTC-Warning index plane

As the new longitudinal safety index, the collision risk in TTC-Warning index plane can be described as Figure 2.8.

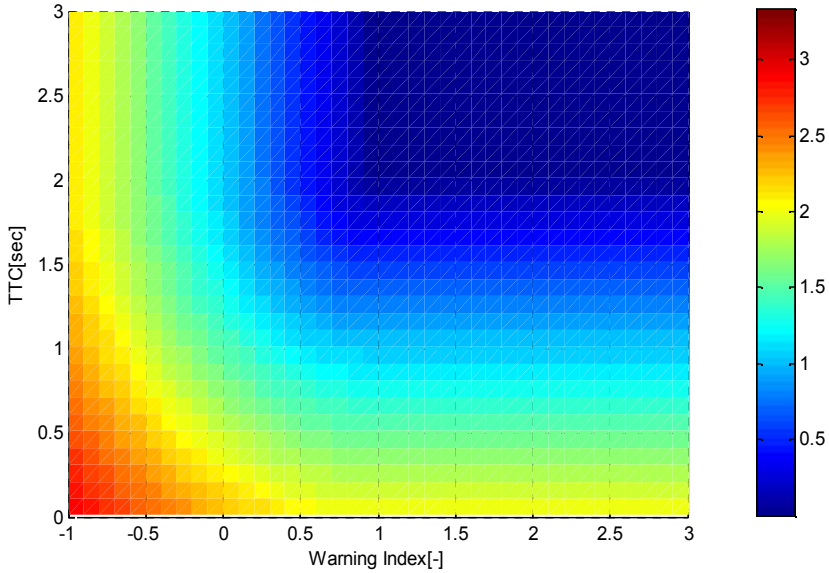

Figure 2.8. Collision risk level of the new safety index in TTC-Warning index plane

Because of the new longitudinal safety index was normalized in terms of TTC and Warning index, if the new longitudinal safety index indicates the '1', it means that vehicle need to operate the maximum deceleration to prevent the rear-end collision by braking maneuver. Therefore, the proposed advanced braking algorithm was designed to operate the braking inputs as the new longitudinal safety index values proportionally.

$$u_{des} = \begin{cases} 0 & if \quad S_{Longi} \le 0 \\ a_{\max} \cdot S_{Longi} & elseif \quad S_{Longi} > 0 \end{cases} \tag{2.11}$$

2.3 Safety Threshold for the New Longitudinal Safety Index

2.2.1 TTC based safety monitoring

To define the control mode in point of the TTC, physical threshold for the crash avoid can be obtained as Last Point To Steer (LPTS) and Last Point To Brake (LPTB).

A. Last Point To Steer (LPTS)

LPTS means that last point to avoid the crash by normal steering input and it can be defined as follow:

$$TTC_{LTPS} = \sqrt{\frac{2 \cdot s_y}{a_y}} \tag{2.12}$$

where, s_y is the lateral distance to crash avoidance and a_y is the lateral acceleration value which is generated in lane-change driving situation.

Through the experimentation, the driver's lane change characteristics are obtained [Lee 11]. Lane change test data were collected not only under the severe situation of collision avoidance but also general experimental lane change situation under the normal safety situation. And both experiments are conducted in several driving speeds; 40, 60, 80, 100kph. From the experimental test data, human drivers perform a lane change maneuvering with uniform level of lateral acceleration peak. As the driving situation changes, maximum values

of lateral acceleration have different values.

To find relation with lane change pattern and driving speed, data in emergency situation are analyzed. Steering angle has higher amplitude at high speed as shown in Figure.2.9-(a). On the other hand, data such as lateral acceleration has similar tendency regardless of the driving speed as shown in the Figure.2.9-(b). On average, the peak of lateral acceleration has the value around 2m/s2 and the total time of lane change has constant value.

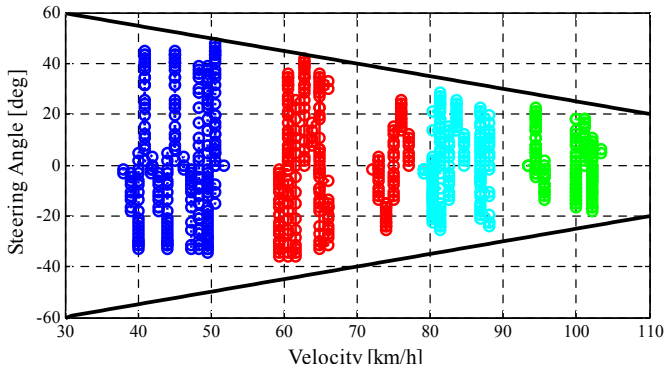

(a) Steering Angle

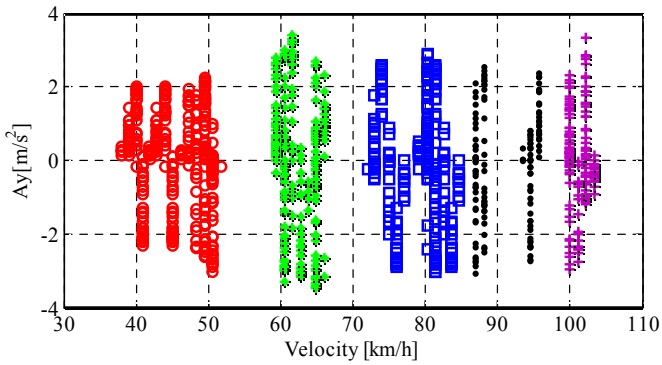

(b) Lateral Acceleration

Figure 2.9 Driver's Steering Characteristics under Different Speed Conditions

Comparing to the normal (not emergency) lane change data, lateral acceleration have higher amplitude in emergency situation as shown in Figure.2.10. In emergency situation, human drivers use 2m/s² as the average maximum lateral acceleration. On the other hand, in normal situation, human drivers use 1m/s² as the average maximum lateral acceleration.

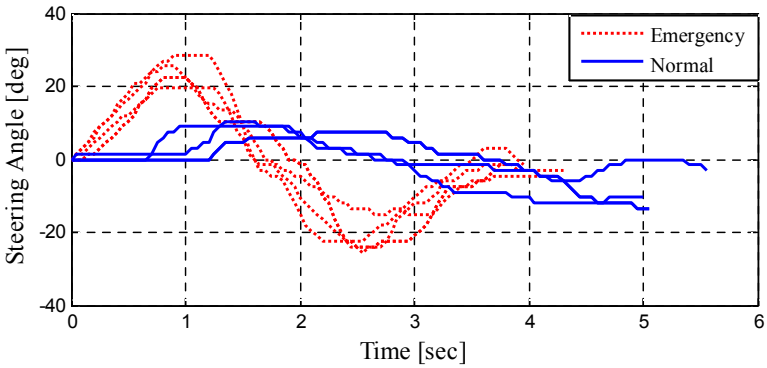

(a) Steering Angle

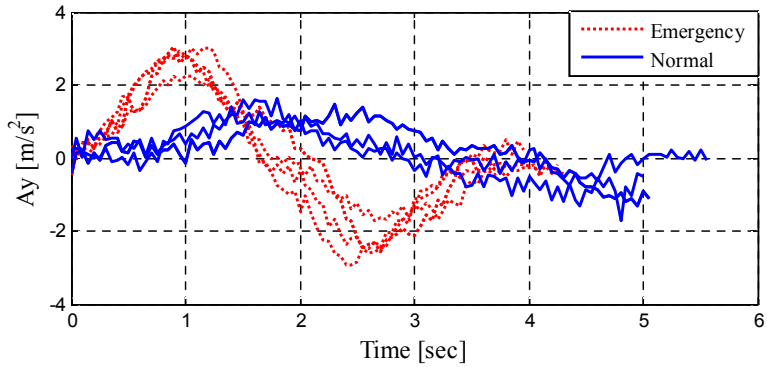

(b) Lateral Acceleration

Figure 2.10 Driver's Steering Characteristics under Different Driving Situations

From the collected data, Last Point To Steer in Emergency driving case and

Last Point To Steer in normal driving case can be defined.

$LPTS_{Emergency}$ and $LPTS_{Normal}$ defined as follow:

$$TTC_{LTPS_{Emergency}} = \sqrt{\frac{2 \cdot s_y}{a_{y,Emergency}}}$$
$$TTC_{LTPS_{Normal}} = \sqrt{\frac{2 \cdot s_y}{a_{y,Normal}}} \quad (2.13)$$

where, sy is the lateral distance to crash avoidance and $a_{y,Emergency}$ is the lateral acceleration value which is generated in emergency lane-change driving situation and $a_{y,Normal}$ is the lateral acceleration in normal lane-change driving situation.

B. Last Point To Brake (LPTB)

LPTB is defined as last point to avoid rear-end collision by braking maneuver. LPTB is defined as:

$$TTC_{LPTB} = \frac{d_{br}}{v_{rel}} \quad (2.14)$$

where, d_{br} is the braking distance and v_{rel} is relative velocity.

The braking distance is the distance that the car travels from the moment that the brakes are applied to the moment that the car stops. The total distance travelled from themoment that the driver perceives the emergency to when the car stops consists of two parts:

- Thinking distance: the distance travelled before the driver actually starts braking.

- Braking distance: the distance the car then travels before coming to rest.

Therefore, in the case of braking distance in normal deceleration (i.e. not emergency braking situation), braking is obtained as:

$$d_{br_{normal}} = v_{rel} \cdot t_{thinking} + v_{rel} \cdot t_{brake} - \frac{v_{rel}^{2}}{2a_{x,normal}} \tag{2.15}$$

where, $t_{thinking}$ is thinking time, t_{brake} is delay time caused by braking actuator and $a_{x,normal}$ is deceleration value in braking.

Also, TTC of the LPTB for partial braking is obtained as:

$$TTC_{LPTB_{normal}} = \frac{d_{br_{normal}}}{v_{rel}} = \frac{v_{rel} \cdot t_{thinking} + v_{rel} \cdot t_{brake} - \frac{v_{rel}^{2}}{2a_{x,normal}}}{v_{rel}} = t_{thinking} + t_{brake} - \frac{v_{rel}}{2a_{x,\max}} \tag{2.16}$$

In the case of braking distance in normal deceleration (i.e. not emergency braking situation), deceleration level could be defined from analysis of manual driving data collected in normal driving condition. From the experimental test data, longitudinal acceleration characteristics with respect to velocity can be obtained. As shown in Figure.2.11, acceleration data was gathered a rhomb-like shape.

In the case of emergency braking in AEB algorithm, because braking decision making to brake is operated by ECU process, Thinking distance value is not needed to consider. Instead, deceleration using is assumed as maximum value. Therefore, braking distance for LPTB in emergency situation is defined as:

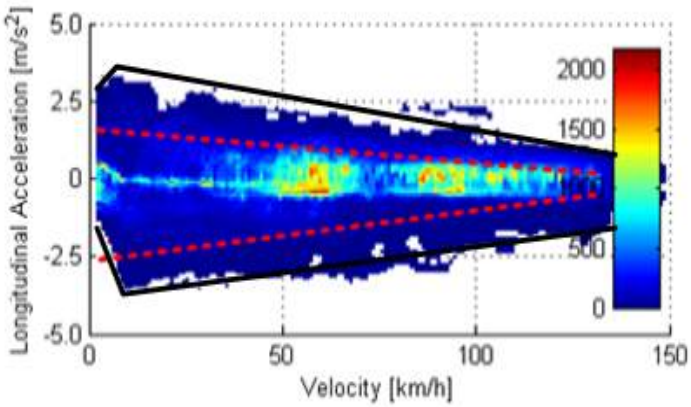

Figure 2.11. Longitudinal Acceleration – Velocity Relation

$$d_{br} = v_{rel} \cdot t_{brake} - \frac{v_{rel}^{2}}{2a_{x,\max}} \tag{2.17}$$

where, and $a_{x,\max}$ is maximum deceleration value.

Also, TTC of the LPTB for emergency braking is obtained as:

$$TTC_{LPTB_{emergency}} = \frac{d_{br}}{v_{rel}} = \frac{v_{rel} \cdot t_{brake} - \frac{v_{rel}^{2}}{2a_{x,\max}}}{v_{rel}} = t_{brake} - \frac{v_{rel}}{2a_{x,\max}} \tag{2.18}$$

C. Threshold Values of the TTC for Braking Control

Threshold values in terms of TTC can be determined by using LPTS and LPTB as defined in previous section. From the definition, distance of the LPTB and LPTS can be draw in Figure 2.12.

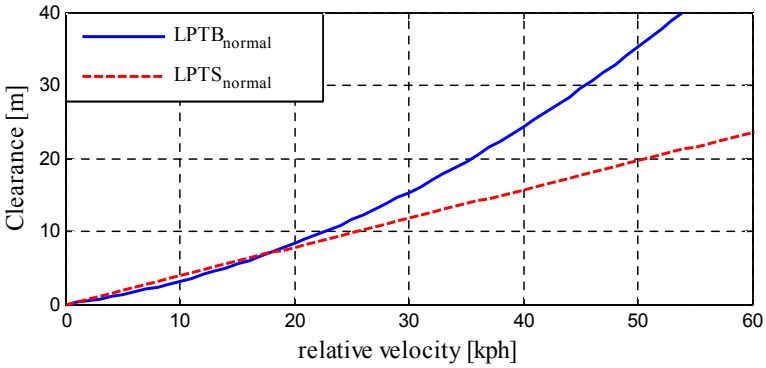

(a)LPTB and LPTS in normal braking/steering situation

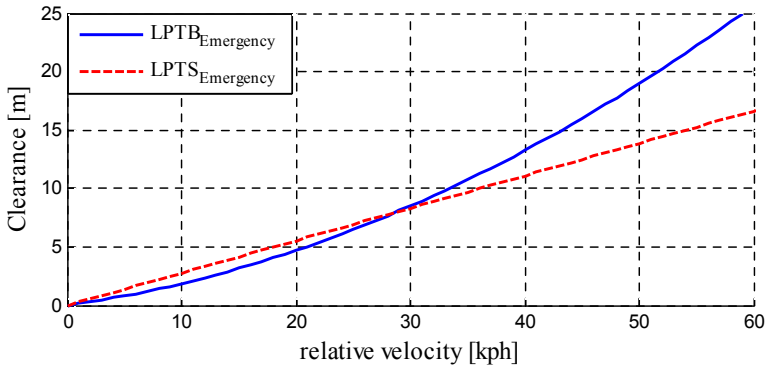

(b) LPTB and LPTS in emergency braking/steering situation

Figure 2.12 Threshold values of the TTC in normal braking for the AEB algorithm

The partial braking threshold value was set as minimum values between LPTB and LPTS in normal driving situation to guarantee the driver's control intention. Likewise, the emergency braking threshold value to be set as minimum values between LPTB and LPTS in emergency driving situation.

Table 2.4 Control Threshold values of the TTC for the AEB algorithm

Control Threshold	Values
$TTC_{warning}$	$TTC = 2\sec$
$TTC_{partial\,braking}$	$Min\left(TTC_{LPTB_{normal}}, \mathrm{TTC}_{LPTS_{normal}}\right)$
$TTC_{emergency\,braking}$	$Min\left(TTC_{LPTB_{emergency}}, \mathrm{TTC}_{LPTS_{emergency}}\right)$

2.2.2 Warning Index based safety monitoring

To divide the control mode in the lower-level controller, threshold value for warning index is set to be two levels: 'Safety threshold' and 'Warning threshold'.

A. Emergency Threshold

The 'Emergency threshold' value means that driver should be start to braking avoid the rear-end collision. If the warning index value is zero, it means that clearance of the driving situation is last point to avoid the rear-end collision by braking maneuver.

$$x = \frac{c - d_b}{d_w - d_b} = 0 \qquad (2.19)$$
$$\therefore c = d_b \approx LPTB$$

B. Safety Threshold

The 'Safety threshold' means the value of which driver starts to feel fear for

driving situation. To calculate the safety threshold value in terms of the warning index, we assume the steady car following situation. In the steady car following situation, relative velocity can be assumed as zero, the warning index can be expressed as follow:

$$x = \frac{c - d_b}{d_w - d_b}$$

$$\begin{cases} d_b = v_{rel} \cdot T_{s,delay} + f(\mu) \cdot \left[\dfrac{v_s^{\,2} - (v_s - v_{rel})^2}{2 \cdot a_{\max}} \right] = 0 \\ d_w = d_b + v_s \cdot T_{h,delay} = v_s \cdot T_{h,delay} \end{cases} \tag{2.20}$$

$$x = \frac{c}{v_s \cdot T_{h,delay}} \tag{2.21}$$

By analysis of the manual driving data in normal car-following situation, we confirm that vehicles clearance about preceding vehicle had tended to maintain linear combination of velocity and normal time-gap.[6]

$$c = \tau \cdot v_s + c_0 \tag{2.22}$$

where, C0 means minimum clearance and τ is the linear coefficient. The linear coefficient can be obtained as Table.2.5.

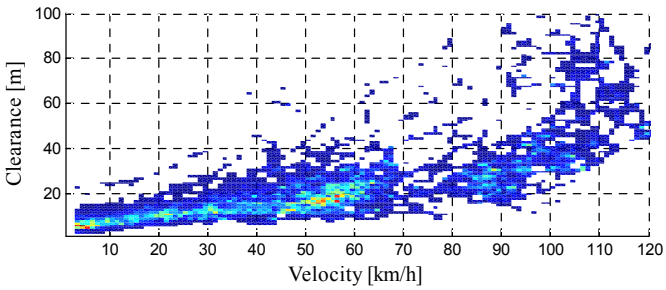

Figure 2.13 Clearance and Velocity relation in the steady car-following situation

Table 2.5 Linear coefficient of the Time gap in Car following situation

Following-Data (15 person, 342min)					
Index-Percentile	5%	25%	Mean	75%	95%
Linear coefficient [s]	0.72	1.07	1.36	1.69	2.27

From the under 5 percentile's linear coefficient, the safety threshold value of the warning index can be obtained as:

$$x = \frac{\tau \cdot v_s}{v_s \cdot T_{h,delay}} = \frac{\tau}{T_{h,delay}} \tag{2.23}$$

C. Threshold Values of the Warning Index for Emergency Braking

The threshold to monitor the safety level of the driving condition in point of Warning index is set as two level: safe level and emergency level. From the previous discussion, Threshold values are determined as Table 2.6.

Table 2.6 Control Threshold values of the Warning Index for the AEB algorithm

Control Threshold	**Values**
x_{safe}	$\frac{\tau}{T_{h,delay}}$
$x_{Emergency}$	0

Chapter 3

Sensor Information Analysis and Environment Information based Longitudinal Safety Control Algorithm

The vehicle longitudinal safety control algorithm for collision avoidance using environment information and a sensor information have been proposed in this chapter. Analysis of the tire-road friction influence and the friction estimation module was described in this chapter. By using the estimated tire-road friction information, safety monitoring was conducted. For robust control mode decision, the RADAR sensor and the vision sensor data was analyzed. The simple static theory and Kalman filter by using the measurement noise is used in this research. By using the expected error, the threshold of each safety index was determined for the safety monitoring of the driving situation.

3.1 Environment Information for Vehicle Longitudinal Safety Control

Tire-road friction influences the ability of tires to generate steering, traction, and braking forces and thus affects vehicle motion. Knowledge of the friction coefficient of the road is thus important for the design and analysis of vehicle control systems, especially active safety systems [Ahn 11].

When friction is unknown, the design of the safety system is usually conservative, resulting in reduced performance.The braking capacity of vehicles changes with adverse environmental conditions, gradual wear of components and highway topology, etc.

In order to maintain longitudinal safety capacity, it is imperative that the braking capabilities of subject vehicle in the system be conservatively estimated. Also, it is also necessary that be estimated its influences as closely as possible to its actual environmental condition[Yi 02].

There is a significant amount of research in tire/road friction modeling.

The model given in [[Bakker 87]], known as the ‘‘magic formula’’, gives a good approximation to experimental results of the relationship between friction coefficient and longitudinal slip, and is widely used in automotive research and industries.

As Dugoff tire model[Dugoff 69], longitudinal tire force varies depending on vertical load and slip ratio, and tire-road friction coefficient. But in real driving situation, slip ratio is not easily predicted. To make control strategy for the

active safety system, it is required to predict vehicle motion and tire-road friction coefficient.

According to the experimental tire-road friction coefficient test, friction coefficient is measured differently depending on vehicle speed, tire pressure, tire type and tire wear. These factors have complex behavior and the associated variables that influence this behavior are difficult to measure.

James[James 05] measured sliding friction coefficient with regard to tire pressure on tire of two types and reported that sliding friction coefficient on wet asphalt road is influenced by vehicle speed, tire pressure, and tire wear. Tire-road friction coefficient is decreased as vehicle speed is increased on wet asphalt road. And tire pressure affect also on tire-road friction coefficient. This experiment was done with special tire mounting equipment. Because the experimental results didn't represent slip ratio of wheel, it was not identified how slip ratio is affected by road condition. This experimental result can be considered in real braking performance expectation. For specific safety system, this type of tire road friction coefficient variation data by road condition and variation can be more important than tire-road friction estimation method.

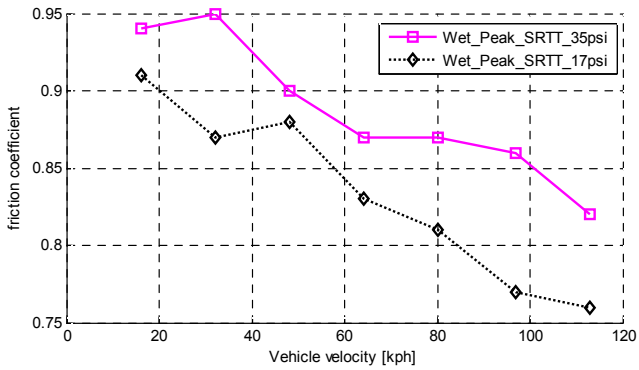

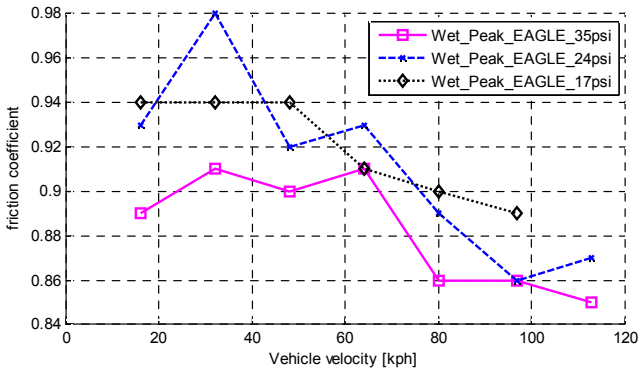

Figure 3.1 Friction coefficient On Wet Asphalt(derived from [James 05])

This experiment was done with special tire mounting equipment. Because the experimental results didn't represent slip ratio of wheel, it was not identified how slip ratio is affected by road condition. This experimental result can be considered in real braking performance expectation. For specific safety system, this type of tire road friction coefficient variation data by road condition and variation can be more important than tire-road friction estimation method.

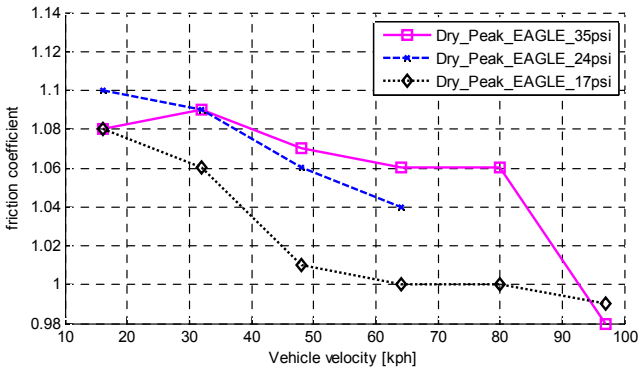

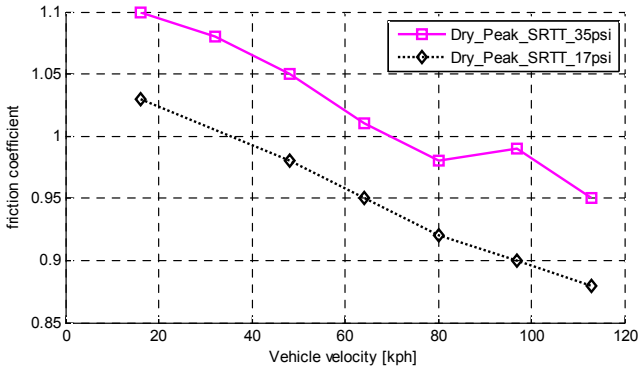

Figure 3.2 Friction coefficient on dry asphalt(derived from [James 05])

C. R. Carlson[Carlson 05] studied about longitudinal stiffness change with temperature and tire pressure and tire wear, vertical load and wet asphalt. Table 3.1 represents longitudinal stiffness change with various conditions. Nominal condition for test is nominal tire pressure, driver only and no tire wear. Test vehicle is 1999 Mercedes E320 with stock installed variable reluctance antilock braking system(ABS) sensors.

The tire pressure is an important factor of the friction coefficient estimation considering both experimental results. Carlson's Experimental result represent that longitudinal stiffness can vary largely with regard to tire wear and tire pressure. Reduced tread by wear is an important factor. Severely wear tire has higher longitudinal stiffness and lower friction coefficient than tire which not wear.

Table 3.1 Longitudinal stiffness change with various conditions(derived from [Carlson 05])

Experimental Condition				Longitudinal Stiffness Change	
Road	Pressure	Tire Tread	Weight	Performance	Winter
Dry	Changed by heat	Full	Driver only	-17%	-21%
Dry	-10%	Full	Driver only	17%	15%
Dry	-20%	Full	Driver only	29%	28%
Dry	nominal	2.5[mm] wear	Driver only	34%	91%
Dry	nominal	Full	Driver +200[kg]	13%	7%
Dry	nominal	Full	Driver +400[kg]	60%	42%
Wet	Nominal	Full	Driver only	4%	-2%

S. Yamazaki's[Yamazaki 97] experiment supports the effect of the tire parameter on the tire-road friction coefficient. Tire wear affects the longitudinal stiffness and the cornering stiffness than the dry/wet condition in that research.

Drum type tire test machine was used to experiment. The longitudinal stiffness on the wet asphalt road was larger than the longitudinal stiffness on the dry asphalt road. But the maximum friction coefficient on the wet asphalt was smaller than the maximum friction coefficient on the dry asphalt. Because the wear condition of the tires was not same in those two experiments, the experimental result is not the good sample for the friction coefficient.

These various parameters to affect tire-road friction force are also considered in real driving situation. As James's study, the longitudinal friction force on the tire is also influenced by the vehicle speed and tire pressure, tire type and wear. And these parameters are difficult to measure except the tire pressure. It is required to attain the table of the tire-road friction coefficient with tire parameters and slip-ratio for the accurate estimation. And the method to measure the tire parameters are required to be devised.

3.2 Tire Force Estimation

Tire-forces and tire-road friction coefficient information are crucial in vehicle dynamics control such as a vehicle stability control (VSC), a smart cruise control and a collision avoidance, etc. However these are difficult or very expensive to measure directly.

Cho[Cho 11] estimated tire-road friction coefficient using IMM of 3 friction coefficient models. Cho propose a tire force estimator for the vertical, longitudinal and lateral tire forces of each wheel. From the estimated longitudinal/lateral tire forces, the tire-road friction coefficient estimators were designed using a multiple model (MM) filter method with the Dugoff - tire model. Figure 3.5 shows the proposed tire-road friction coefficient estimation architecture.

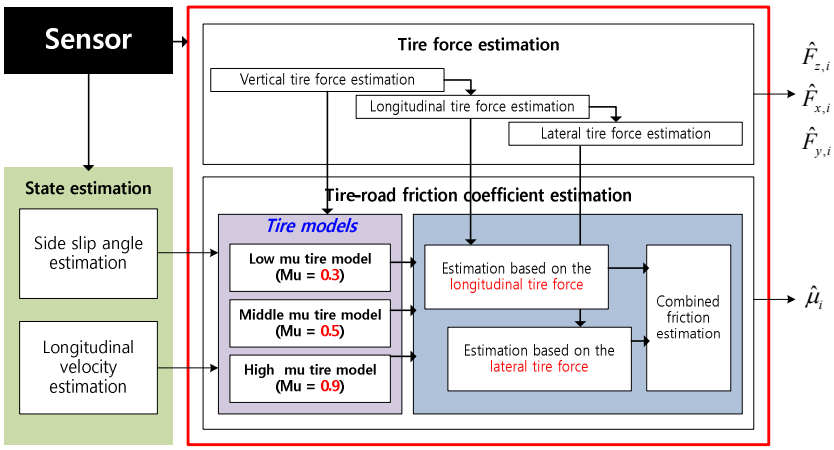

Figure 3.5 Tire information estimation architecture (derived from [Cho 11])

The tire force estimator is designed for the vertical, the longitudinal and lateral tire forces of each wheel. The estimator consists of the vertical tire force estimation, the shaft torque estimation, the longitudinal tire force estimation, the lateral tire force estimation and the combined tire force estimation. Figure 3.6 shows the Cho's proposed tire force estimation algorithm.

The vertical tire force can be simply estimated using the longitudinal/lateral accelerations and roll sates. In the case of the shaft torque, estimator has been designed by using the turbine torque, the turbine angular velocity and the wheel angular velocity. Also, the longitudinal and lateral tire force can be estimated by the wheel angular velocity, the lateral acceleration, the longitudinal acceleration and the yaw rate. From each estimated tire force, the combined tire force estimator can be designed by using the measurements such as the longitudinal acceleration, the lateral acceleration and the yaw rate.

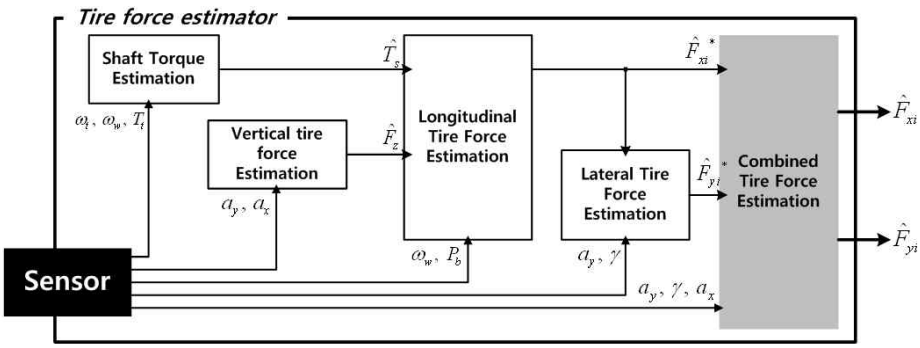

Figure 3.6 Structure of the tire force estimator (derived from [Cho 11])

The tire-road friction coefficient estimated based on estimated longitudinal and lateral tire forces. The longitudinal tire force-based estimator and the lateral

tire force-based estimator use an MM filter method with a Dugoff-tire model. In order to design the MM filter, the various Dugoff-tire models were designed by taking differences in road friction coefficients. Through a comparison of the tire forces at the Dugoff -tire models and the estimated tire forces, the tire-road friction coefficient can be estimated.

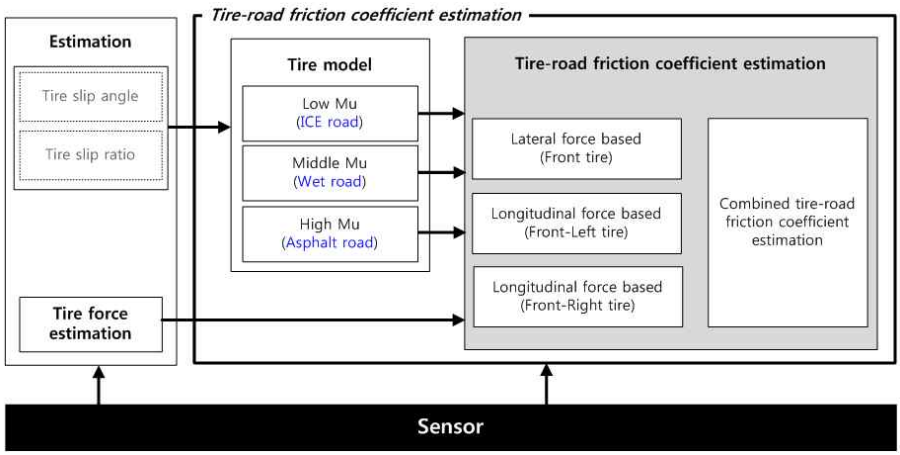

Figure 3.7 Tire-road friction coefficient estimator scheme (derived from [Cho11])

From Cho's tire-road friction estimating, the estimator cannot estimate the reliable friction coefficient value when the absolute value of the slip ratio is less than 0.02 in longitudinal motion. This means that in the normal steady driving situation without lateral motion Cho's tire-road friction estimation cannot guarantee the reliable friction value. Therefore, we assumed that in the case of normal steady-straight driving condition, the tire-road friction estimation could not update the estimated value. Instead, the given friction parameter are updated

by using the temperature sensor and rain sensor signal. For example, in case of the rainy day in the summer and steady-straight driving condition, updated tire-road friction value is set as 0.5 which is well-known tire-road friction coefficient of the wet asphalt.

3.3. Safety Monitoring by using the environment information

This chapter discusses friction for enhanced longitudinal safety control algorithm design. Friction potential affects the maximum predicted accelerations of vehicle longitudinal dynamic. A new method is introduced for collision avoidance and mitigation calculations, with an emphasis on effective computing.

3.3.1 Influence of the Tire-road friction on TTC based safety monitoring

The use of friction information in longitudinal safety control had not been concerned for algorithm development generally. A common approach is to include friction potential in vehicle chassis control such as ESC, UCC for calculation of maximum lateral force or maximum tire force. However, in the case of collision mitigation control, tire-road friction is very important factor in braking capacity.

The tire-road friction simply affects maximum accelerations. Maximum acceleration value is can be defined as

$$a_{\max} = \mu \cdot g \tag{3.1}$$

The braking distance values which was defined in previous chapter is re-derived as:

$$
\begin{aligned}
d_{br} &= v_{rel} \cdot t_{brake} - \frac{v_{rel}^{2}}{2a_{x,\max}} \\
&= v_{rel} \cdot t_{brake} - \frac{v_{rel}^{2}}{2 \cdot \mu \cdot g}
\end{aligned}
\tag{3.2}
$$

Therefore, the braking distance values by tire-road friction easily can be described as following Figure 3.8.

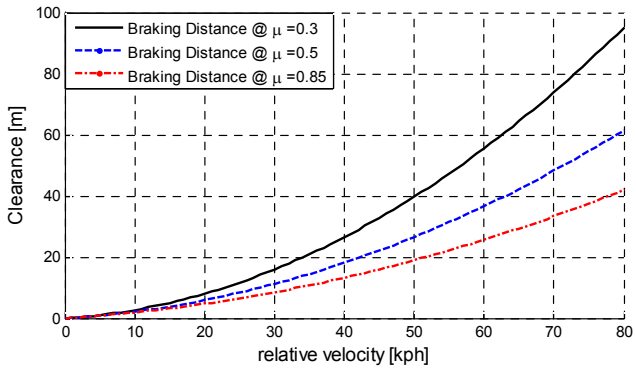

Figure 3.8 Braking distance by tire-road friction

From the definition of TTC of the LPTB for emergency braking, Eq.(3.3) can be defined.

$$
\begin{aligned}
TTC_{LPTB_{emergency}} &= \frac{d_{br}}{v_{rel}} \\
&= t_{brake} - \frac{v_{rel}}{2 \cdot \mu \cdot g}
\end{aligned}
\tag{3.3}
$$

Also, the braking distance in normal braking can be defined same approach as

$$
\begin{aligned}
d_{br_{normal}} &= v_{rel} \cdot t_{thinking} + v_{rel} \cdot t_{brake} - \frac{v_{rel}^{2}}{2a_{x,normal}} \\
&= v_{rel} \cdot t_{thinking} + v_{rel} \cdot t_{brake} - \frac{\mu_{normal}}{\hat{\mu}} \cdot \frac{v_{rel}^{2}}{2 \cdot a_{x,normal}}
\end{aligned}
\tag{3.4}
$$

$$TTC_{LPTB_{normal}} = \frac{d_{br_{normal}}}{v_{rel}} = t_{thinking} + t_{brake} - \frac{\mu_{normal}}{\hat{\mu}} \cdot \frac{v_{rel}}{2 \cdot a_{x,normal}} \tag{3.5}$$

Likewise, the last point to steer can be effected by tire-road friction. If the vehicle movement is generated only lateral direction, the maximum lateral acceleration can be defined as

$$a_{y,\max} = \mu_y \cdot g \tag{3.6}$$

Because the distance of the LPTS was defined by square-root of the lateral displacement and lateral acceleration, the LPTS can be defined as

$$d_{LTPS} = v_{rel} \cdot \sqrt{\frac{2 \cdot s_y}{a_{y,\mu}}} \tag{3.7}$$

From the definition, influence of tire-road in the LPTS is

$$\eta_\mu = \frac{1}{\sqrt{\mu}} \tag{3.8}$$

and, the TTC of the LPTS is derived as

$$TTC_{LPTS} = \frac{TTC_s(\hat{\mu})}{TTC_s(\mu_{\text{nominal}})} \cdot TTC_{LPTS_{\text{nominal}}} = \sqrt{\frac{\mu_{\text{nominal}}}{\hat{\mu}}} \cdot TTC_{LPTS_{\text{nominal}}} \tag{3.9}$$

Distance of the LPTS by tire-road friction is described in Figure 3.9.

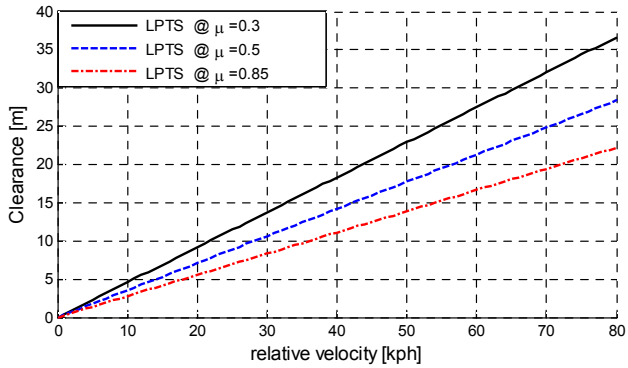

Figure 3.9 Distance of the LPTS by tire-road friction

3.3.2 Tire-road friction based control threshold of TTC

By using the collected obstacle information and tire-road friction information, TTC of the LPTB and LPTS for partial braking and emergency braking situation can be defined as:

Table 3.2 LPTB and LPTS for partial braking and emergency braking situation

PARTIAL BRAKING	EMERGENCY BRAKING
$TTC_{LPTB_{normal}} = t_{thinking} + t_{brake} - \frac{\mu_{normal}}{\hat{\mu}} \cdot \frac{v_{rel}}{2 \cdot a_{x,normal}}$	$TTC_{LPTB_{emergency}} = t_{brake} - \frac{v_{rel}}{2 \cdot \mu \cdot g}$
$TTC_{LTPS_{Normal}} = \sqrt{\frac{\mu_{\text{nominal}}}{\hat{\mu}} \cdot \frac{2 \cdot s_y}{a_{y,Normal}}}$	$TTC_{LTPS_{Emergency}} = \sqrt{\frac{\mu_{\text{nominal}}}{\hat{\mu}} \cdot \frac{2 \cdot s_y}{a_{y,Emergency}}}$

Likewise the previous Chapter, the partial braking threshold value defined as minimum values between re-defined LPTB and LPTS in normal driving case

to guarantee the driver's control intention. Also, the emergency braking threshold value set as minimum values between LPTB and LPTS in emergency driving situation with tire-road friction influence considered.

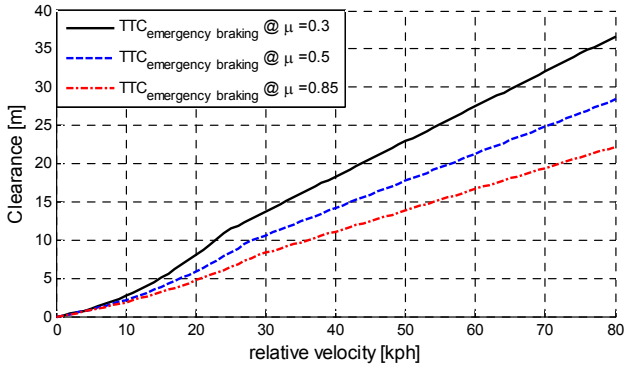

Figure 3.10 Threshold for Emergency Braking by tire-road friction

3.3.3 Influence of the Tire-road friction on Warning Index based safety monitoring

In the case of the Warning Index, from the definition of the index, the warning index can be influenced by using the maximum deceleration. The warning-critical and braking-critical distances for the warning index are defined with maximum deceleration as follows:

$$d_{br} = v_{rel} \cdot t_{brake} - \frac{v_{rel}^{\ 2}}{2a_{x,\max}} = v_{rel} \cdot t_{brake} - \frac{v_{rel}^{\ 2}}{2 \cdot \mu \cdot g}$$
$$d_{w} = v_{s} \cdot t_{thinking} + v_{rel} \cdot t_{brake} - \frac{v_{rel}^{\ 2}}{2 \cdot \mu \cdot g} \qquad (3.10)$$

Therefore, the warning index can be derived as

$$x = \frac{c - d_{br}}{d_w - d_{br}} = \frac{c - \left(v_{rel} \cdot t_{brake} - \frac{v_{rel}^{\ 2}}{2 \cdot \mu \cdot g} \right)}{v_s \cdot t_{thinking}} \tag{3.11}$$

In the various driving situation, estimated braking distance by using the tire-road friction can detect the collision risk earlier.

In the case of the warning Index, it was assumed that SV and PV decelerate maximum acceleration in the same road condition. Therefore, if the relative velocity is zero which means steady following situation, the warning index is not effected by tire-road friction. However, in the case of braking situation or facing to the stop-preceding vehicle with low friction condition, braking distance could be increased and warning index will be lower than same driving situation with high friction condition.

3.4. Sensor Information for Vehicle Longitudinal Safety Control

In order for the longitudinal safety system to provide a positive and beneficial influence towards the reduction of potential crashes, it is critical that the safety system has the ability to correctly identify the vehicle, pedestrian and object targets in the vehicle's path [Zhang 06]. Environmental sensors have a limited field of view and uncertainty or error terms this usually leads to unexpected control failure or poor control performance.

The solution to this problem relies primarily on the longitudinal safety system's sensing system ability to estimate the detection range, relative speed, etc. between the subject vehicle and all other appropriate targets.

The in-path target identification and discriminating them from out of path objects are technically very complex and challenging task in collision avoidance system [Zhang 06]. However, in this context, the resultant information from sensor and in-path target estimation algorithm is assumed to be obtained.

The range and range rate information of other vehicles and/or objects around the subject vehicle can be measured by sensors RADAR and/or cameras in real time. Two kinds of sensors are used in this study. One is a RADAR (Radio Detection And Ranging) sensor and the other is a vision sensor.

3.4.1 RADAR (Radio Detection And Ranging)

The Radar is currently the most widely adopted sensing technology for automotive ranging applications. The RADAR is a system that uses electromagnetic waves to identify the range, direction, or speed of both moving and fixed objects such as aircraft, ships, motor vehicles, weather formations, and terrain.

In this technology the distance from the object is calculated through the echoes that are sent back from the object. The determination of the position of an object is done through the time-of-flight and angle measurement. In process of time-of-flight measurements, electromagnetic energy is sent toward objects and the returning echoes are observed. The measured time difference and the speed of the signal allow calculating the distance to the object. The Speed measurement is made through the Doppler-effect. The base of Doppler-effect is change of wavelength due to the changing gap between waves. Although the amount of signal returned is tiny, radio signals can easily be detected and amplified [Bayless 14].

RADAR sensors are also known to have sufficient robustness to function reliably under harsh environmental conditions for extended periods of time.

3.4.2 Vision (Camera Sensor)

Vision systems use one or several cameras together with a microprocessor to perform image processing. Since they operate in the visible light region, their capabilities are similar to that of our own eyes. A camera based sensor is used to detect car/obstacle in front of the subject vehicle. Camera based

longitudinal safety system are typically used for medium range, medium field of view detection. The camera system can be charge coupled device (CCD) based or Complementary Metal Oxide Semiconductor (CMOS) based [Bayless 14].

In their basic single camera configuration video imagers cannot provide ranging information. However, using the principle of triangulation coupled to obstacle recognition routines, the images viewed by camera systems may be processed to facilitate identification of obstacles and their range. Such systems provide good obstacle and environmental recognition using non-intrusive means.

Cameras are able to provide information about target position for slow moving vehicles. They are capable of detecting targets even when placed at a distance from the region to be monitored. However, cameras placed in this fashion, provides poor longitudinal position accuracy.

3.4.3 Sensing Results

An experiment was performed by using the test vehicle which is equipped RADAR and vision sensor system for measuring the range and range-rate to the proceeding vehicle under driving conditions. Data is collected at various range and relative velocity with constant speed of target vehicle.

Figure 3.11 Test Vehicle for sensor system

In many cases, due to road curvatures, other vehicles, uneven road surfaces relative lateral position and lateral movement, the measurement range distribution might be different. Also, the exact reflection point is uncertain since the azimuth angle is not very exact, so for medium distances the main reflection point may be located on different parts of the car. Hence, test data was collected in the test road without other vehicle or obstacle.

Table.3.3 Initial Setting Condition for Sensor data collection

	SV	**PV**
Initial Speed	30/35/40/45/50/55/60/65/70/75/80kph	20kph
Initial Range	70m	

The lateral displacement of the longitudinal centerline of the subject vehicle relative to the longitudinal centerline of the target vehicle kept less than 1,0 m.

The subject vehicle cruises behind the preceding vehicles in initial vehicle speed. The initial speed and range of SV and PV are set as Table.3.3. To validate the sensor detection performance, the GPS-based device, RT-Range, is used to measure the reference of the range and range rate data. The RT-Range device uses RT-3000 which is precision GPS device, and is attached by the test vehicle independently.

In Figure 3.12, range error in vehicle test is depicted. As shown in Figure 3.12, vision sensor and RADAR sensor has similar detection error pattern within the 10m range. On the other hand, range error of the Vision sensor is bigger than the RADAR sensors over the 10m range situation.

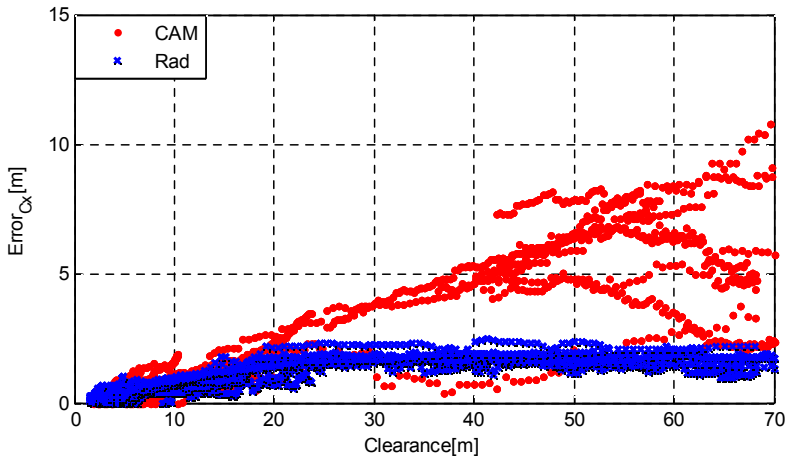

Figure 3.12. Range Error vs. Range

In Figure 3.13, detected positions of targets at SV initial speed is 80km/h and are depicted. A black-circle mark represents the GPS signal and a red-dotted mark is from the Vision sensor. A blue-square mark is represent the RADAR

sensor signal. As shown in Figure 3.13(b), collected range data of the RADAR sensors has biased error values. In the case of the Vision sensor, it was observed as non-uniform error pattern.

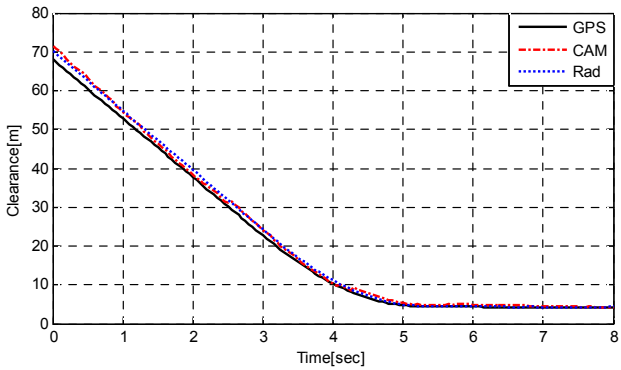

(a) Real driving data - Range: Vs=80km/h and Vp=20 km/h

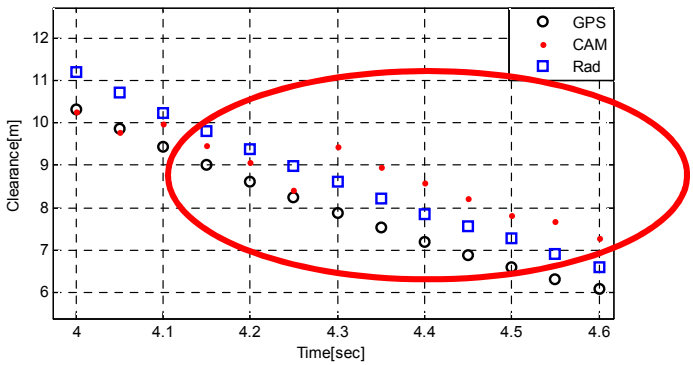

(b) Zoom-in: Range data

Figure 3. 13 Range data of RADAR sensor and Vision sensor

The exact appearance of the error will vary with many factors such as target vehicle, sensor and traffic situation. In this research, the range error of both sensors are assumed as the Gaussian noise. The variance and standard deviation

value of range error is presented in Figure 3.14 and Figure 3.15.

As mentioned above, the vision sensor and RADAR sensor has similar detection error variance pattern within the 10m range (RADAR: 0.77 vs. Vision: 1.13). In the case of over the 20m range situation, range error of the Vision sensor is bigger than the RADAR sensors. The variation and the standard deviation of the RADAR senor is saturated in specific values as clearance values increasing.

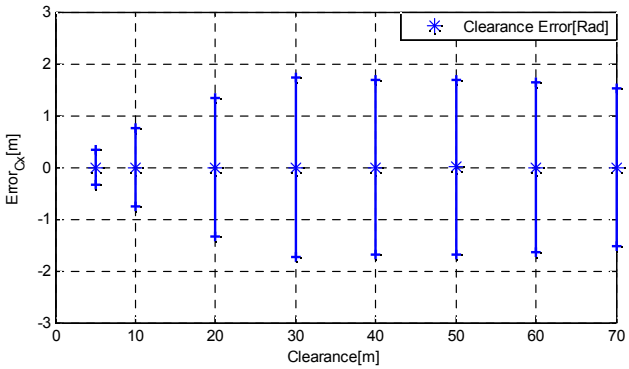

Figure 3.14 Range Error vs. Range : RADAR sensor

Table 3.4 Variance and Standard deviation value of range error: RADAR sensor

C(m)	***5m***	***10m***	***20m***	***30m***	***40m***	***50m***	***60m***	***70m***
Var(σ^2)	0.12	0.59	1.81	2.98	2.87	2.86	2.82	2.32
Std(σ)	0.35	0.77	1.35	1.73	1.70	1.70	1.65	1.52

On the other hand, the Vision sensor's variation and standard deviation

values are increasing proportionally with clearance values increasing until 50m.

By using these results, the range error distribution can be modeled as Table 3.6.

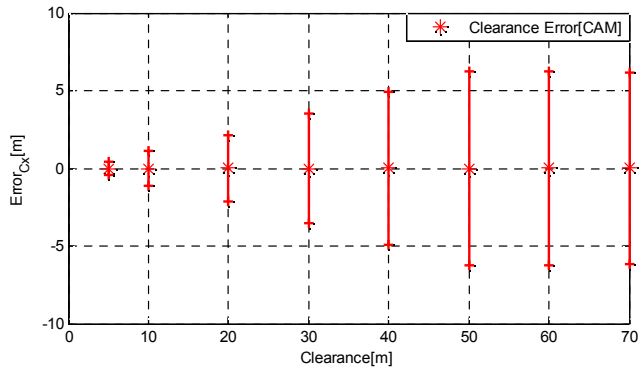

Figure 3.15 Range Error vs. Range: Vision sensor

Table 3.5 Variance and Standard deviation value of range error: Vision sensor

C(m)	*5m*	*10m*	*20m*	*30m*	*40m*	*50m*	*60m*	*70m*
Var(σ^2)	0.24	1.28	4.64	12.29	24.27	38.52	38.80	37.58
Std(σ)	0.46	1.13	2.15	3.50	4.92	6.21	6.23	6.13

Table 3.6 Standard deviation value of range error

	5m	*10m*	*20m*	*30m*	*40m*	*50m*	*60m*	*70m*
σ_{RAD}	0.35	0.77	1.35	1.70	1.70	1.70	1.70	1.70
σ_{Vision}	0.46	1.13	2.15	3.50	4.92	6.20	6.20	6.20

In Figure 3.16, range rate error is depicted. As shown in Figure 3.16, distribution of the error in the case of the RADAR sensor has smaller variance than the Vision sensor.

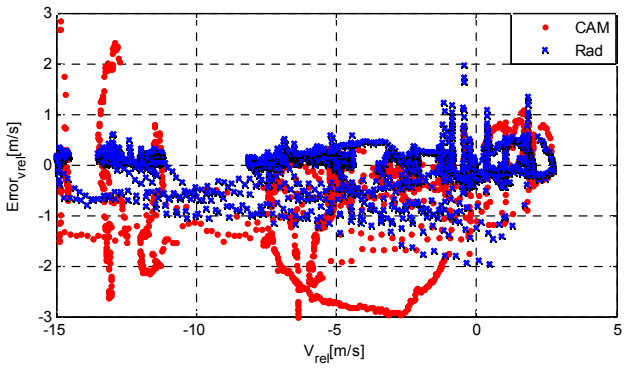

Figure 3.16. Range rate Error vs. Range rate

Measured relative velocity of targets at SV initial speed is 80km/h is depicted in Figure 3.17. As shown in Figure 3.17, the RADAR sensors has similar with reference data. However, in the case of the Vision sensor, biased error values are observed.

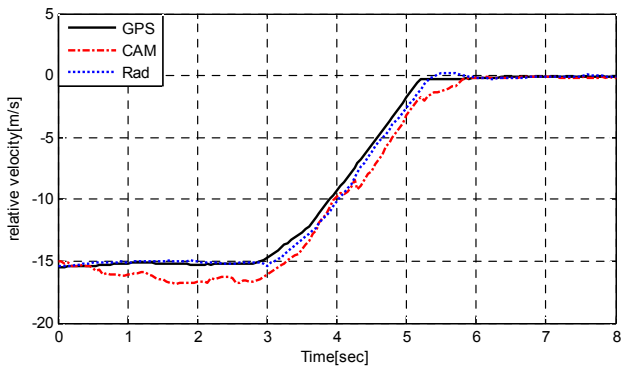

Figure 3. 17 Range rate data of RADAR sensor and Vision sensor

The variance and standard deviation value of range error is presented in Figure 3.18 and Figure 3.19. As mentioned above, the range rate error of the RADAR sensor has similar values with GPS data for overall relative velocity range. Regardless of velocity range, range rate error are remained within ±1m/s. On the other hand, the Vision sensor's variation and standard deviation values are bigger than the RADAR sensor. Particularly, in the case of relative velocity between SV and PV is over the 5m/s, the range rate error occurred ±3m/s.

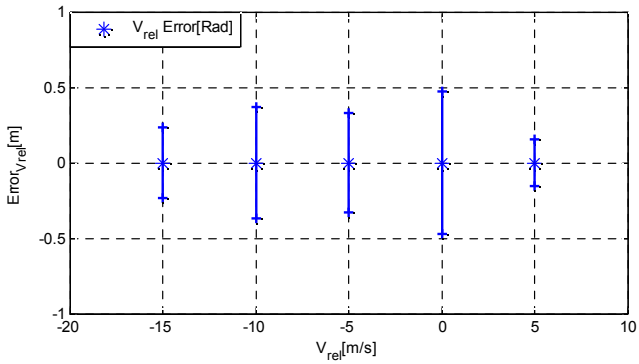

Figure 3.18 Range rate Error vs. relative velocity: RADAR sensor

Table 3.7 Variance and Standard deviation value of range rate error: RADAR sensor

Vrel(m/s)	***- 15m/s***	***- 10m/s***	***- 5m/s***	***0m/s***	***5m/s***
Var(σ^2)	0.05	0.14	0.11	0.22	0.02
Std(σ)	0.23	0.37	0.33	0.47	0.15

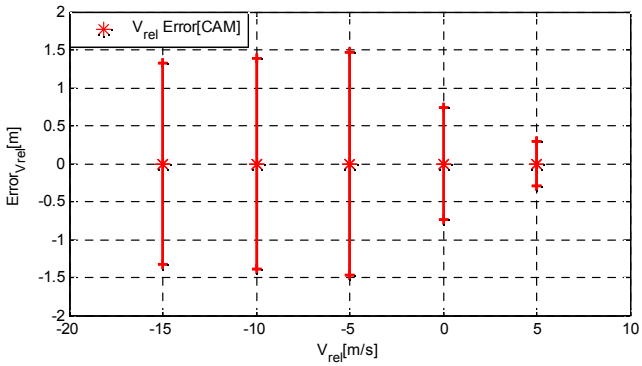

Figure 3.19 Range rate Error vs. relative velocity: Vision sensor

Table 3.8 Variance and Standard deviation value of range rate error: Vision sensor

Vrel(m/s)	***-15m/s***	***-10m/s***	***-5m/s***	***0m/s***	***5m/s***
Var(σ^2)	1.77	1.93	2.13	0.54	0.01
Std(σ)	1.33	1.39	1.46	0.73	0.30

Similarly to the range error, the range rate error distribution can be modeled involves these results as Table 3.9.

Table 3.9 Standard deviation value of range error

Vrel(m/s)	***-15m/s***	***-10m/s***	***-5m/s***	***0m/s***	***5m/s***
σ_{RAD}	0.4	0.4	0.4	0.4	0.4
σ_{Vision}	1.4	1.4	1.4	0.7	1.4

3.5 Sensor Data Fusion

In this research, the RADAR sensor and the Vision sensor is used. The key advantage of RADAR-vision fusion systems is that robust verified data is guaranteed and used by the algorithms in order to provide a solid foundation for the resulting applications. The research states that cameras are known for their capability of measuring the angles to the outline of a target precisely, and for providing a classification of objects. On the other hand, range and speed measurements are less accurate, for which the laser compensates. The fusion module receives detections and tracks from the individual sensors and merges them to a consistent environment description. This includes classification of the observed objects and their dynamics. This is due to the fact that the data is derived from two separate sensors and fused, matched and then approved. In order to fuse two sensor data, the simple static theory and Kalman filter is used in this research.

Before describing the sensor data fusion, the assumption of the sensor data have to be defined first. The following is on the assumption that each sensor selects the primary target to control in own process, and sensor data fusion is conducted by using the selected primary target data. In order words, target selection and tracking is not included in research area.

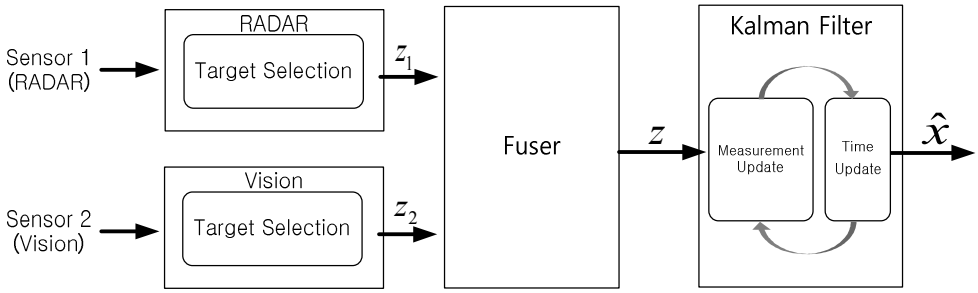

Figure 3.20. Assumption of the sensor data fusion

3.5.1 Assumption of the sensor data fusion

As shown in previous section, the vision sensor and RADAR sensor has different resolution by the clearance and velocity and detectable range. Also, each measured signal include the uncertainty or error value. To enhance the reliability of the measured signal, the simple static theory is used.

A. Clearance data

To fuse the measured clearance data, the measurement state of clearance by each sensor can be defined as follows:

$$\begin{aligned} Radar&: z_{11} = x_1 + v_{11} \quad v_{11} \sim N(0, \sigma_{11}) \\ CAM&: z_{21} = x_1 + v_{21} \quad v_{21} \sim N(0, \sigma_{21}) \end{aligned} \tag{3.12}$$

The estimated state of the clearance can be obtained by using the measurement state and proportion gain as follow:

$$\hat{x}_1 = k_1 \cdot z_{11} + k_2 \cdot z_{21} \tag{3.13}$$

Also, estimation error is defined as

$$\tilde{x}_1 \triangleq \hat{x}_1 - x_1 \tag{3.14}$$

The first goal of the estimated state is making the unbiased estimation which means estimation error should be zero. From the Eq (3.14), estimation error can be derived as propagation gains and mean values of each sensor noise as follow:

$$\begin{aligned} E\left[\tilde{x}_1\right] &= E\left[\hat{x}_1 - x_1\right] \\ &= E\left[\left(k_1 \cdot z_{11} + k_2 \cdot z_{21}\right) - x_1\right] \\ &= E\left[\left\{k_1\left(x_1 + v_{11}\right) + k_2\left(x_1 + v_{21}\right)\right\} - x_1\right] \\ &= \left(k_1 + k_2 - 1\right) \cdot E\left[x_1\right] + k_1 \cdot E\left[v_{11}\right] + k_2 \cdot E\left[v_{21}\right] \\ &= 0 \end{aligned} \tag{3.15}$$

Mean values of each sensor noise is zero in the definition of the Eq.(3.12), a correlation between proportion gain k_1 and k_2 can be derived as:

$$k_1 + k_2 = 1 \tag{3.16}$$

The second object of the estimated state is minimizing the variance of the estimated state. The estimated variance can be defined as follow:

$$\sigma_{\hat{x}_1}{}^2 \triangleq E\left[\left(\hat{x} - \hat{x}_m\right)^2\right] = E\left[\tilde{x}^2\right] \tag{3.17}$$

$$\begin{aligned} E\left[\tilde{x}^2\right] &= E\left[\left(\hat{x} - x\right)\left(\hat{x} - x\right)\right] \\ &= E\left[\left\{k_1\left(x_1 + v_{11}\right) + k_2\left(x_1 + v_{21}\right) - x_1\right\}^2\right] \\ &= E\left[\left\{k_1 x_1 + k_1 v_{11} + k_2 x_1 + k_2 v_{21} - x_1\right\}^2\right] \\ &= E\left[\left\{\left(k_1 + k_2 - 1\right) x_1 + k_1 v_{11} + k_2 v_{21}\right\}^2\right] \end{aligned} \tag{3.18}$$

Using the correlation between propagation gain as Eq.(3.16), the estimated variance can be transformed as follows:

$$
\begin{aligned}
\sigma_{\hat{x}_1}{}^2 &= E\left[\left(k_1 \cdot v_{11} + k_2 \cdot v_{21}\right)^2\right] \\
&= E\left[\left(k_1{}^2 \cdot v_{11}{}^2 + 2 \cdot k_1 \cdot k_2 \cdot v_{21} \cdot v_{11} + k_2{}^2 \cdot v_{21}{}^2\right)\right] \\
&= k_1{}^2 \cdot E\left[v_{11}{}^2\right] + 2 \cdot k_1 \cdot k_2 \cdot E\left[v_{21}\right] \cdot E\left[v_{11}\right] + k_2{}^2 \cdot E\left[v_{21}{}^2\right]
\end{aligned}
\tag{3.19}
$$

Because of each sensor measurement is uncorrelated, the estimated variance is defined as

$$
\sigma_{\hat{x}_1}{}^2 = k_1{}^2 \cdot \sigma_{11}{}^2 + k_2{}^2 \cdot \sigma_{21}{}^2 \tag{3.20}
$$

To define propagation gain for minimizing the estimated variance, we can derive Eq.(3.21)

$$
\begin{aligned}
&\min_{k_1}\left(\sigma_{\hat{x}_1}{}^2\right) = \min_{k_1}\left(E\left[\left(\tilde{x}^2\right)\right]\right) \\
&\rightarrow \frac{\partial}{\partial k_1} E\left[\left(\tilde{x}^2\right)\right] = 0 \\
&\therefore 2k_1\sigma_{11}{}^2 - 2\left(1 - k_1\right)\sigma_{21}{}^2 = 0
\end{aligned}
\tag{3.21}
$$

From the Eq.(3.21), propagation gain for best estimated state can be obtained as follow:

$$
k_1 = \frac{\sigma_{21}{}^2}{\sigma_{11}{}^2 + \sigma_{21}{}^2}, \quad k_2 = \frac{\sigma_{11}{}^2}{\sigma_{11}{}^2 + \sigma_{21}{}^2} \tag{3.22}
$$

Hence, the fused estimated state of the clearance data can be defined as

$$
\hat{x}_1 = \frac{\sigma_{21}{}^2}{\sigma_{11}{}^2 + \sigma_{21}{}^2} \cdot z_{11} + \frac{\sigma_{11}{}^2}{\sigma_{11}{}^2 + \sigma_{21}{}^2} \cdot z_{21} \tag{3.23}
$$

From the analysis results in previous chapter, variance of the measured clearance data can be described as Figure 3.21.

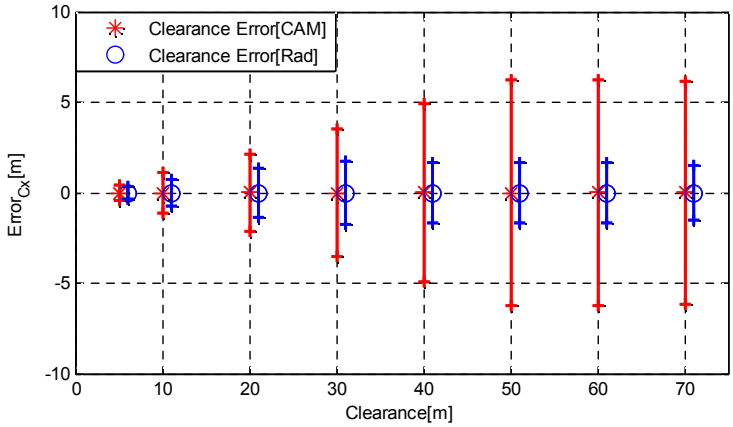

Figure.3.21 variance of the measured clearance data

By using the estimated state equation and analysis of standard deviation values of each sensor, the proportion gain can be set as Table 3.10.

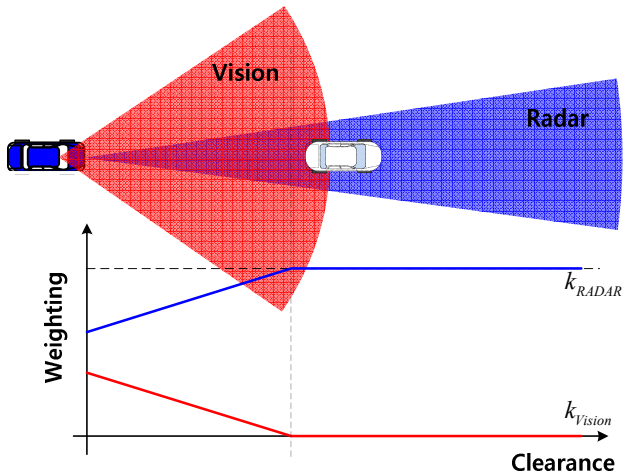

Figure.3.22 Weighting Factor and Sensor Detection Range

Table 3.10 Standard deviation value and propagation gain for estimated clearance

	5m	*10m*	*20m*	*30m*	*40m*	*50m*	*60m*	*70m*
σ_{RAD}	0.35	0.77	1.35	1.70	1.70	1.70	1.70	1.70
σ_{Vision}	0.46	1.13	2.15	3.50	4.92	6.20	6.20	6.20
k_1	0.6	0.7	0.7	0.80	0.9	1	1	1
k_2	0.4	0.3	0.3	0.20	0.1	0	0	0

B. Relative velocity data

To fuse the measurement data, the measurement state of relative velocity by each sensor can be defined as follows:

$$\begin{aligned} &Radar: z_{12} = x_2 + v_{12} \quad v_{12} \sim N(0, \sigma_{12}) \\ &CAM: z_{22} = x_2 + v_{22} \quad v_{22} \sim N(0, \sigma_{22}) \end{aligned} \tag{3.24}$$

The identical conception of the clearance measurement, the fused estimated state defined as propagation gain and each measurement state as

$$\hat{x}_2 = k_3 \cdot z_{12} + k_4 \cdot z_{22} \tag{3.25}$$

From the analysis of the estimation state for clearance, the fused relative velocity estimated state can be defined as

$$\hat{x}_2 = \frac{\sigma_{22}^{\ 2}}{\sigma_{12}^{\ 2} + \sigma_{22}^{\ 2}} \cdot z_{12} + \frac{\sigma_{12}^{\ 2}}{\sigma_{12}^{\ 2} + \sigma_{22}^{\ 2}} \cdot z_{22} \tag{3.26}$$

Variance of the measured relative velocity data can be described as Figure 3.23.

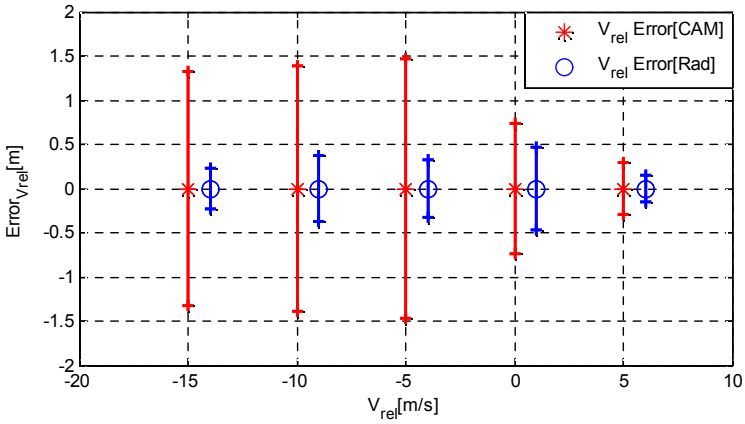

Figure.3.23 variance of the measured relative velocity data

By using the estimated state equation and analysis of standard deviation values of each sensor, the proportion gain can be set as Table 3.11.

Table 3.11 Standard deviation value and propagation gain for estimated relative velocity

Vrel(m/s)	***-15m/s***	***-10m/s***	***-5m/s***	***0m/s***	***5m/s***
Var(σ^2)	0.4	0.4	0.4	0.4	0.4
Std(σ)	1.4	1.4	1.4	0.7	1.4
k_3	0.9	0.9	0.9	0.6	0.9
k_4	0.1	0.1	0.1	0.4	0.1

3.5.2 Filtering of the fused measurement signal by Kalman filter

The fused measurement signal is filtered and estimated by using the Kalman

filter. The filter estimates the process state at some time and then obtains feedback in the form of measurements.

$$\begin{aligned} x(k+1) &= F \cdot x(k) + v(k) \\ z(k) &= H \cdot x(k) \end{aligned} \tag{3.27}$$

A longitudinal relative distance, lateral relative distance and longitudinal relative velocity can be measured by RADAR. Originally lateral relative velocity can be obtained from RADAR, but this signal is very noisy. Even if it is filtered, it can't be applied. So lateral relative velocity is considered as no measured signal and estimated by Kalman filtering.

As such, the equations for the Kalman filter fall into two groups. One is time update equations and the other is measurement update equations. The time update equations are responsible for projecting forward the current state and error covariance estimates to obtain the a priori estimates for the next time step. The measurement update equations are responsible for the feedback, i.e. for incorporating a new measurement into the a priori estimate to obtain an improved a posteriori estimate. The time update equations can also be thought of as predictor equations, while the measurement update equations can be thought of as corrector equations. The specific equations for time update are presented as follows:

$$\begin{aligned} x_m(k) &= F \cdot x_p(k-1) \\ P_m(k) &= F \cdot P_p(k-1) \cdot F^T + Q \end{aligned} \tag{3.28}$$

Notice that the time update equations project the state and covariance estimates forward. The specific equations for the measurement update are presented as follows:

$$
\begin{aligned}
M(k) &= H \cdot P_m(k) \cdot H^T + V \\
K(k) &= P_m(k) \cdot H^T \cdot M(k)^{-1} \\
x_p(k) &= x_m(k) + K(k)\big(z(k) - H \cdot x_m(k)\big) \\
P_p(k) &= P_m(k) - K(k) \cdot H \cdot P_m(k)
\end{aligned}
\tag{3.29}
$$

The first task during the measurement update is to compute the Kalman gain, K. The next step is to actually measure the process to obtain z(k), and then to generate an a posteriori state estimate by incorporating the measurement as in (3.28). The final step is to obtain a posteriori error covariance estimate via equation (3.29). After each time and measurement update pair, the process is repeated with the previous a posteriori estimates used to project or predict the new a priori estimates. Figure 3.24 offers a complete picture of the operation of the filter.

By the way, clearance and relative velocity signal which was obtained from filtering process as previous chapter can be as covariance matrix of the Kalman filter as;

$$
\begin{aligned}
\sigma_{\hat{x}_1}{}^2 &= P_{11} \\
\sigma_{\hat{x}_2}{}^2 &= P_{22}
\end{aligned}
\tag{3.30}
$$

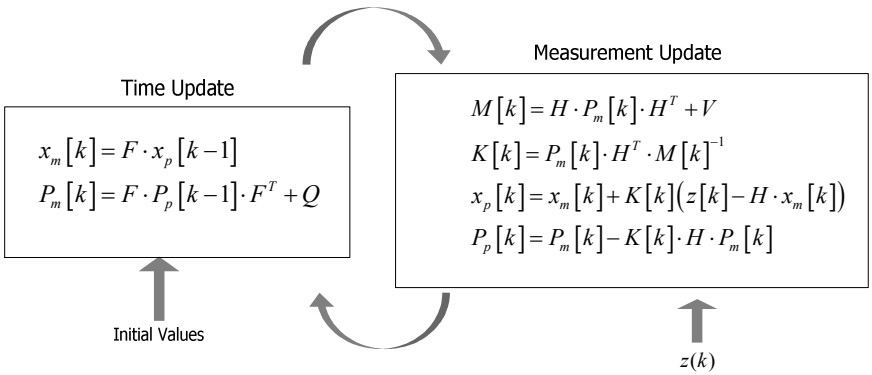

Figure 3.24 Scheme of a Kalman Filter

3.6. Control Mode Decision by using the Fused Sensor Data

For robust control mode decision by using the measurement noise, simple definition of the deviation of the function was used. In the case of determination of a quantity function f , which depends on several variables, the error in f can be defined with standard deviation of the measured variables.

For a single-variable function $f(x)$, the deviation in f can be related to the deviation in x using calculus:

$$\delta f = \left(\frac{df}{dx}\right)\delta x \tag{3.31}$$

Thus, taking the square and the average:

$$\overline{\delta f}^2 = \left(\frac{df}{dx}\right)^2 \overline{\delta x^2} \tag{3.32}$$

And using the definition of standard deviation, we get

$$\sigma_f = \left|\frac{df}{dx}\right| \sigma_x \tag{3.33}$$

In the case where f depends on two or more variables, the derivation above can be repeated with minor modification. For two variables, $f(x, y)$, we have:

$$\delta f = \left(\frac{\partial f}{\partial x}\right)\delta x + \left(\frac{\partial f}{\partial y}\right)\delta y \tag{3.34}$$

The partial derivative $\frac{\partial f}{\partial x}$ means differentiating f with respect to x holding the other variables fixed. Taking the square and the average, we get the law of

propagation of uncertainty:

$$(\delta f)^2 = \left(\frac{\partial f}{\partial x}\right)^2 (\delta x)^2 + \left(\frac{\partial f}{\partial y}\right)^2 (\delta y)^2 + 2\left(\frac{\partial f}{\partial x}\right)\left(\frac{\partial f}{\partial y}\right)\delta\bar{x}\delta\bar{y} \quad (3.35)$$

If the measurements of x and y are uncorrelated, then $\delta\bar{x}\delta\bar{y} = 0$, and using the definition of standard deviation, we get

$$\sigma_f = \sqrt{\left(\frac{\partial f}{\partial x}\right)^2 \sigma_x^{\ 2} + \left(\frac{\partial f}{\partial y}\right)^2 \sigma_y^{\ 2}} \quad (3.36)$$

3.6.1. Expected Error range of the safety index

Expected error range of the new longitudinal safety index from the measurement noise can be defined. Because the measurements of clearance and relative velocity is variables of the new longitudinal safety index function, the new longitudinal safety index can be express as

$$S_{Longi} = f\left(TTC, TTC_{normal}, TTC_{Emergency}, x, x_{normal}, x_{Emergency}\right)$$
$$= \left[\left(\frac{TTC - TTC_{normal}}{TTC_{Emergency} - TTC_{normal}}\right)^2 + \left(\frac{x - x_{normal}}{x_{Emergency} - x_{normal}}\right)^2\right]^{\frac{1}{2}} \quad (3.37)$$

By using the definition of the standard deviation of filtered measurement signal and two measurement variable in the Equation (3.37), expected error of the Longitudinal Safety Index can be derived as:

$$\sigma_{S_{Longi}} = \sqrt{\left(\frac{\partial f}{\partial x_1}\right)^2 \sigma_{x_1}^{\ 2} + \left(\frac{\partial f}{\partial x_2}\right)^2 \sigma_{x_2}^{\ 2}} \quad (3.38)$$

$$\frac{\partial f}{\partial x_1} = \frac{1}{2}\left[S_{Longitu}\right]^{-\frac{1}{2}} \cdot \left[\frac{2\cdot\frac{x_1}{x_2^{\,2}} - \frac{2\cdot\left(t_{thinking}+t_{brake}\right)}{x_2} + \frac{1}{a_{x,normal}}}{\left(\frac{1}{2a_{x,normal}} - \frac{1}{2a_{x,\max}}\right)^2 \cdot x_2^{\,2} - t_{thinking}\cdot\left(\frac{1}{a_{x,normal}} - \frac{1}{a_{x,\max}}\right)\cdot x_2 + t_{thinking}^{\,2}} + \frac{2}{v_s^{\,2}\cdot\tau_{following}^{\,2}}\cdot x_1 - \frac{2\cdot t_{brake}}{v_s^{\,2}\cdot\tau_{following}^{\,2}}\cdot x_2 - \frac{1}{a_{\max}\cdot v_s^{\,2}\cdot\tau_{following}^{\,2}}\cdot x_2^{\,2} - \frac{2}{v_s\cdot\tau_{following}} \right]$$

$$\frac{\partial f}{\partial x_2} = \frac{1}{2}\left[S_{Longi}\right]^{\frac{1}{2}} \cdot \left[\begin{array}{l} \frac{x_1^{\,2}\cdot -2\cdot x_2^{\,-3} + 2\cdot\frac{1}{2^2 a_{x,normal}^{\,2}}\cdot x_2 - 2\cdot\left(t_{thinking}+t_{brake}\right)\cdot x_1\cdot -1\cdot x_2^{\,-2} - \frac{\left(t_{thinking}+t_{brake}\right)}{a_{x,normal}}}{\left(\frac{1}{2a_{x,normal}} - \frac{1}{2a_{x,\max}}\right)^2 \cdot x_2^{\,2} - t_{thinking}\cdot\left(\frac{1}{a_{x,normal}} - \frac{1}{a_{x,\max}}\right)\cdot x_2 + t_{thinking}^{\,2}} \\ - \frac{\left(x_1^{\,2}\cdot x_2^{\,-2} + \frac{1}{2^2 a_{x,normal}^{\,2}}\cdot x_2^{\,2} - 2\cdot\left(t_{thinking}+t_{brake}\right)\cdot x_1\cdot x_2^{\,-1} - \frac{\left(t_{thinking}+t_{brake}\right)}{a_{x,normal}}\cdot x_2\right)\cdot\left(2\cdot\left(\frac{1}{2a_{x,normal}} - \frac{1}{2a_{x,\max}}\right)^2\cdot x_2\right)}{\left(\left(\frac{1}{2a_{x,normal}} - \frac{1}{2a_{x,\max}}\right)^2 \cdot x_2^{\,2} - t_{thinking}\cdot\left(\frac{1}{a_{x,normal}} - \frac{1}{a_{x,\max}}\right)\cdot x_2 + t_{thinking}^{\,2}\right)^2} \\ + \frac{\left(x_1^{\,2}\cdot x_2^{\,-2} + \frac{1}{2^2 a_{x,normal}^{\,2}}\cdot x_2^{\,2} - 2\cdot\left(t_{thinking}+t_{brake}\right)\cdot x_1\cdot x_2^{\,-1} - \frac{\left(t_{thinking}+t_{brake}\right)}{a_{x,normal}}\cdot x_2\right)\cdot\left(t_{thingking}\cdot\left(\frac{1}{a_{x,normal}} - \frac{1}{a_{x,\max}}\right)\right)}{\left(\left(\frac{1}{2a_{x,normal}} - \frac{1}{2a_{x,\max}}\right)^2 \cdot x_2^{\,2} - t_{thinking}\cdot\left(\frac{1}{a_{x,normal}} - \frac{1}{a_{x,\max}}\right)\cdot x_2 + t_{thinking}^{\,2}\right)^2} \\ -2\cdot\frac{t_{brake}}{v_s^{\,2}\cdot\tau_{following}^{\,2}}\cdot x_1 - 2\cdot\frac{1}{a_{\max}\cdot v_s^{\,2}\cdot\tau_{following}^{\,2}}\cdot x_1\cdot x_2 \\ +4\cdot\frac{1}{2^2\cdot a_{\max}^{\,2}\cdot v_s^{\,2}\cdot\tau_{following}^{\,2}}\cdot x_2^{\,3} + 3\cdot\frac{t_{brake}}{a_{\max}\cdot v_s^{\,2}\cdot\tau_{following}^{\,2}}\cdot x_2^{\,2} \\ +2\cdot\left(\frac{1}{a_{\max}\cdot v_s\cdot\tau_{following}} + \frac{t_{brake}^{\,2}}{v_s^{\,2}\cdot\tau_{following}^{\,2}}\right)\cdot x_2 + 2\cdot\frac{t_{brake}}{v_s\cdot\tau_{following}} \end{array} \right]$$

Expected error of the Longitudinal Safety Index was depicted in Figure 6.

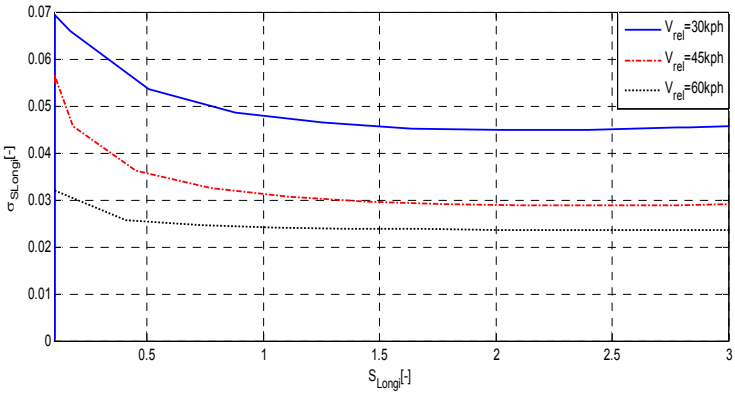

Figure 3.25 Expected error of the Longitudinal Safety Index

3.6.2. Control Mode Decision

From the analysis result of previous section, expected error of safety indices are defined by measurement signals and its variation as follow:

It means that when we set a threshold value for the safety index by using the measured clearance and relative velocity, it contained the uncertainty values which is caused by the measured signal. Therefore, threshold values for safety indices should be considered its expected error.

$$S_{measured} = S_{true} \pm e_S \tag{3.39}$$

The standard deviation of the Safety Index($\sigma_{S_{Longi}}$) for this set of measurements is roughly how far from the average value most of the readings fell. For the true threshold value, approximately 68% of the readings will be within $\sigma_{S_{Longi}}$ of the threshold value by measurement signal value, 95% of the readings will be in the interval $S_{measurement} \pm 2\sigma_{S_{Longi}}$, and nearly all (99.7%) of readings will lie within

$3\sigma_{S_{Longi}}$ from the measurement based threshold value.

Therefore, to set a control mode more safe, threshold values for the control mode selection were consider only positive deviation case, therefore threshold values of each safety index are set as follow:

$$S_{control} = S_{measured} + 3\sigma_{S_{Longi}} \tag{3.40}$$

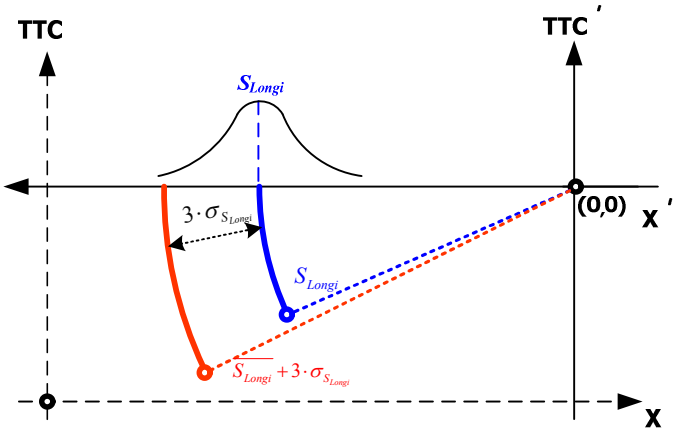

Figure 3.26 Expected error of the Longitudinal Safety Index

Chapter 4

Simulation of the Vehicle Longitudinal Safety Algorithm

The proposed vehicle longitudinal safety algorithm was evaluated through computer simulations using vehicle simulation software, CARSIM and MATLAB/Simulink.

To classify the enhanced safety performance by the proposed longitudinal safety algorithm, two type simulations are conducted to verify the effectiveness of the proposed vehicle longitudinal safety algorithm by the considered information terms as:

1) Fused sensor information based safety algorithm vs. RADAR sensor information based safety algorithm
2) Tire-road friction and fused sensor information based algorithm vs RADAR sensor information based safety algorithm

In these simulations, Simulations for representing a careless driver in normally occurred rear-end collision situation, we assumed that brake control

by the driver was not given in simulated driving situation. Instead, for maintaining the subject vehicle's initial speed or steady following motion until the rear-end collision event occurred, subject vehicle's throttle/brake was considered as controlled for cruise driving. In the case of steering control, wheel steering angle is determined by a driver steering model in the CARSIM software to present human drivers in lane following situation.

Also, AEB algorithm by using the sliding mode control method by Lie was used to compare the robustness of the proposed algorithm.[Lie 14] The sliding mode controller was constructed as:

Error State:

$$\begin{aligned} &\varepsilon = \hat{c} - c_{\min} \qquad where,\ c_{\min} = \tau \cdot v_s + c_0 \\ &\dot{\varepsilon} = v_p - v_s = \hat{v}_{rel} \end{aligned} \tag{4.1}$$

Sliding Surface:

$$S = \dot{\varepsilon} - \lambda_1 \varepsilon - \lambda_2 \int \varepsilon dt \tag{4.2}$$

Desired Acceleration:

$$\begin{aligned} &\dot{S} = \ddot{\varepsilon} - \lambda_1 \dot{\varepsilon} - \lambda_2 \varepsilon = -\beta \operatorname{sgn}(s) \\ &a_s = a_{des} = a_p - \lambda_1 \dot{\varepsilon} - \lambda_2 \varepsilon + \beta \operatorname{sgn}(s) \\ &\quad \therefore a_{des} = -\lambda_1 \cdot \hat{v}_{rel} - \lambda_2 \cdot (\hat{c} - c_{\min}) + \beta \operatorname{sgn}(s) \end{aligned} \tag{4.3}$$

4.1 Simulation with/without fused sensor information for longitudinal safety algorithm

In this section, the behaviors of controlled vehicle by the RADAR sensor information based longitudinal safety algorithm and controlled vehicle by the fused sensor information based longitudinal safety algorithm are presented and compared.

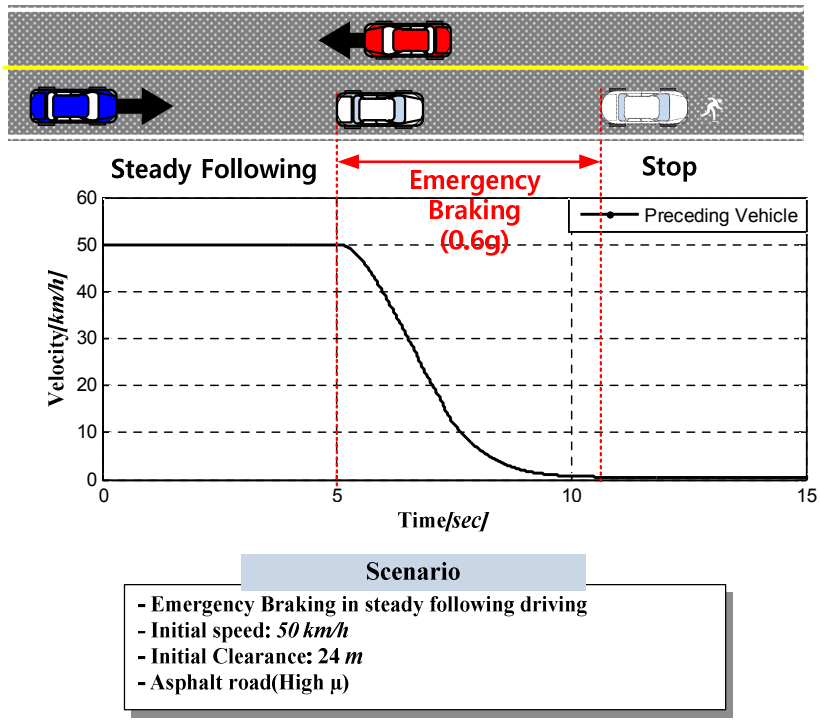

Figure 4.1 Simulation scenario to evaluate the performance of enhanced longitudinal safety: with/without fused sensor information

The simulations with emergency braking vehicle in the straight road was conducted. A lane keeping and a steady following driving was simulated on the dry asphalt road. The initial vehicle speed was set to 50 km/h and driver's additional control inputs were not applied during the simulation. Figure 4.1 shows a simulation scenario that consists of velocity profile, scenario, and driving condition. Since a simulation for the emergency braking situation which could occurred in real driving situation, preceding vehicle's deceleration was assumed as $6\ m/sec^2$.

To classify simulation results by the controlled algorithm, in the case of simulation results by using the fused sensor information based safety algorithm marked as 'With σ' and results of the RADAR sensor information based safety algorithm is named 'Without σ'.

As shown in the velocity profile in Figure 4.2, after the emergency braking of the preceding vehicle started at 5s, clearance between preceding vehicle and subject vehicle is decreased. However, the subject vehicle is maintain the initial speed by assumption that driver was dozing off behind the wheel until the longitudinal safety algorithm operate the braking at 7s.

As shown in Figure 4.2 (c), measured clearance error which was occurred from the sensor model is much smaller in fused clearance error than in RADAR clearance error. Especially, the farther clearance situation, error of the RADAR based system is the bigger as shown in real RADAR system analysis. In the case of relative velocity, error values are similar level in fused and RADAR only case.

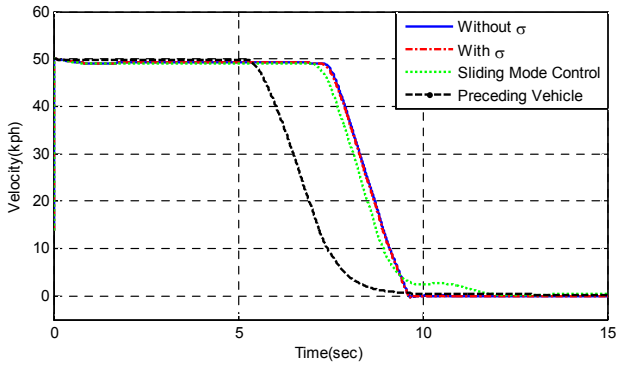

(a) Velocity

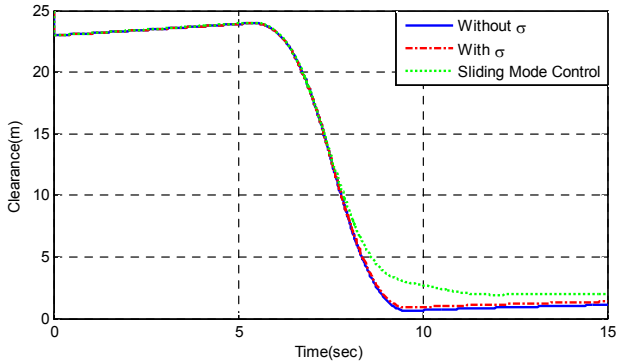

(b) Clearance

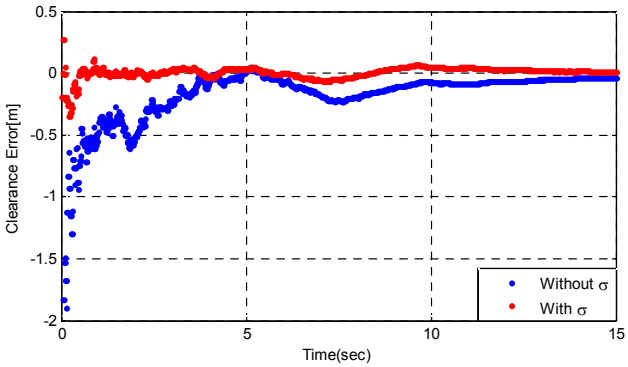

(c) Clearance error

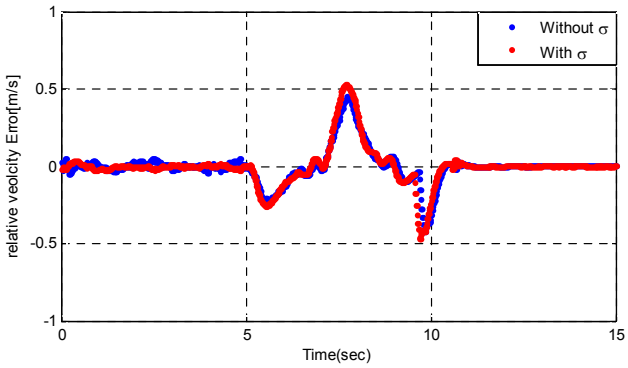

(d) relative velocity error

Figure 4.2 Simulation results: with/without fused sensor information

As decreasing of the clearance and the relative velocity between preceding vehicle and subject vehicle, safety indices values also decreasing rapidly. As shown in Figure 4.3-(a), in the case of the 'without σ', the new safety index is determined by the established control law. Also, safety threshold values for the control mode selection were considered with expected deviation of safety index. As a result, control mode of the 'With σ'case was changed faster than 'Without σ'case about 0.1s. Generally, 0.1s is considered as an effectiveness for control performance. However, in case of vehicle at 50km/h, vehicle move a 1.2m during 0.1s and it could be an essential difference in prevent the rear-end collision. Consequentially, rear-end collision could prevent by both case. However, considering in the warning index-TTC plane, the vehicle state of the 'With σ' is maintained more safe region than 'Without σ' by using sensor information analysis results.

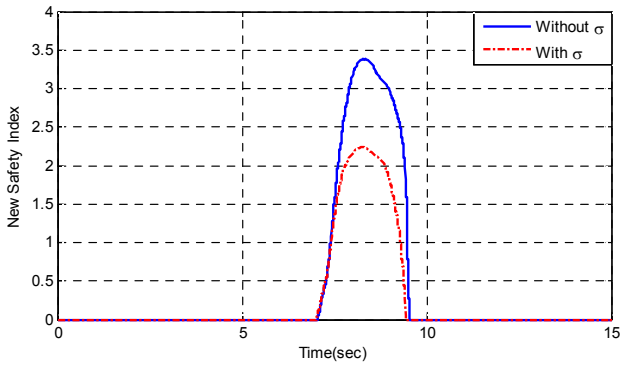

(a) New Safety Index

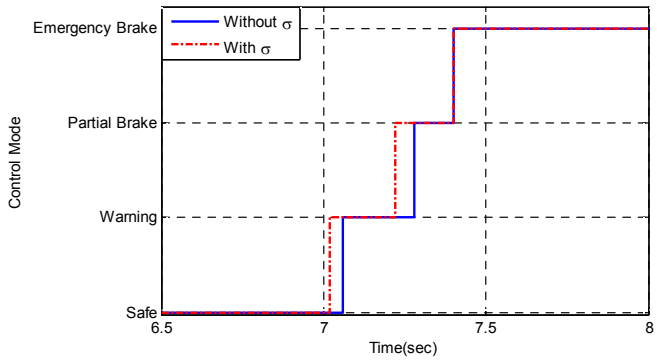

(b) Control Mode

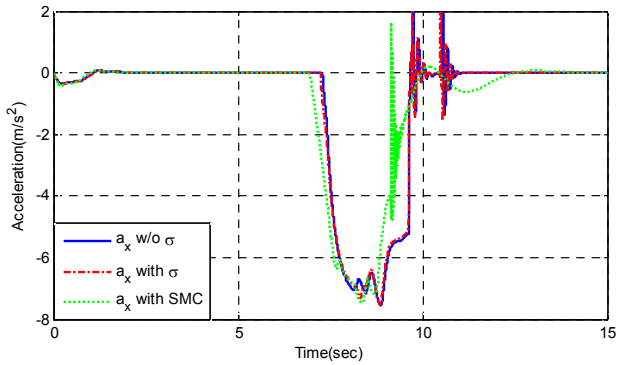

(c) Longitudinal Acceleration

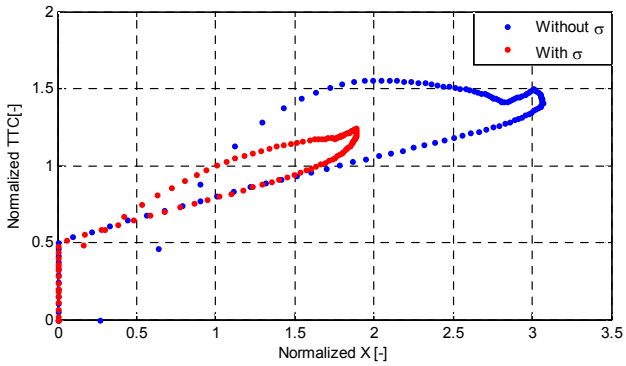

(d) Normalized TTC-Warning Index

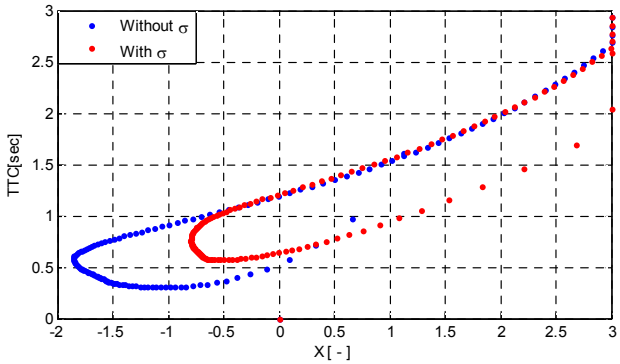

(e) TTC – Warning Index

Figure 4.3 Simulation results: with/without fused sensor information

To confirm the robustness of the 'With σ' case from the sensor uncertainty, the simulation was conducted 100 iteration in the same scenario. As shown in Figure 4.4, the minimum clearance of both case is distributed near 1m. However, the variance and the standard deviation has big different as (0.03 vs 0.01) and (0.17 vs 0.10). Also, in the case of the 'Without σ', rear-end collision couldn't prevent 25 times by the braking of the control algorithm. In contrast, 'With σ' case could prevent rear-end collision in all iteration. From these results, it could

be concluded that proposed longitudinal safety algorithm by using the sensor information analysis could enhanced the longitudinal safety and guarantee the robust capacity to the sensor uncertainty or measurement error.

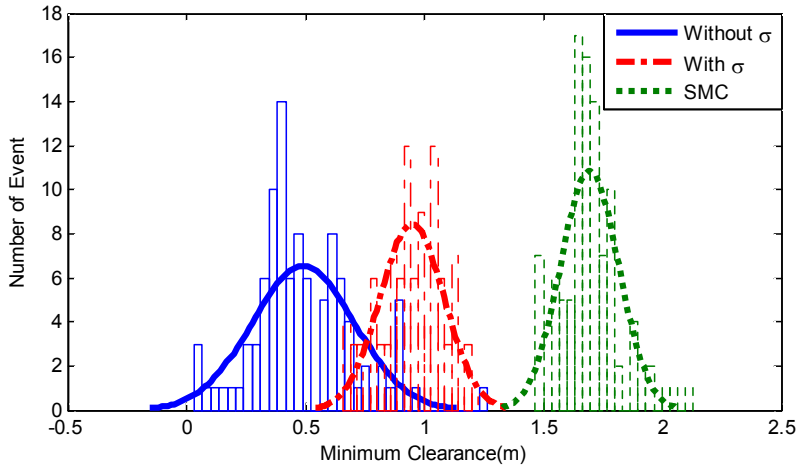

Figure 4.4 Simulation results from 100 iterations:

with/without fused sensor information

Table 4.1 Results of 100 simulation with/without fused sensor information

	Withoutσ	*With σ*	*SMC*
Mean	0.49	0.95	1.69
Variance	0.049	0.017	0.014
Standard Deviation	0.22	0.13	0.12
Number of Crash	6/100	0/100	0/100

Especially, in case of the ‘With σ’, the variation and standard deviation of the minimum clearance is similar with the sliding mode control case. It means that by using the fused sensor signal and filtering method, robustness to the sensor noise uncertainty could be guaranteed as much as sliding mode control method which is well-known robust nonlinear control method.

4.2 Simulation with tire-road friction information for longitudinal safety algorithm

In this section, the behaviors of controlled vehicle by the RADAR sensor information based safety algorithm and controlled vehicle by the tire-road friction and the fused sensor information based longitudinal safety algorithm are presented and compared.

Figure 4.5 Simulation scenario to evaluate the performance of enhanced longitudinal safety: with/without tire-road friction information and sensor information analysis.

The simulations with stopped vehicle in the rainy day was conducted. The initial vehicle speed was set as 50 km/h and driver's additional control inputs were not applied during the simulation. Figure 4.5 shows a simulation scenario that consists of tire-road friction profile, scenario, and driving condition.

To classify simulation results by the controlled algorithm, in the case of simulation results by using the RADAR sensor information based safety algorithm marked as 'Without μ' and results of the tire-road friction and the fused sensor information based longitudinal safety algorithm is named 'With μ'.

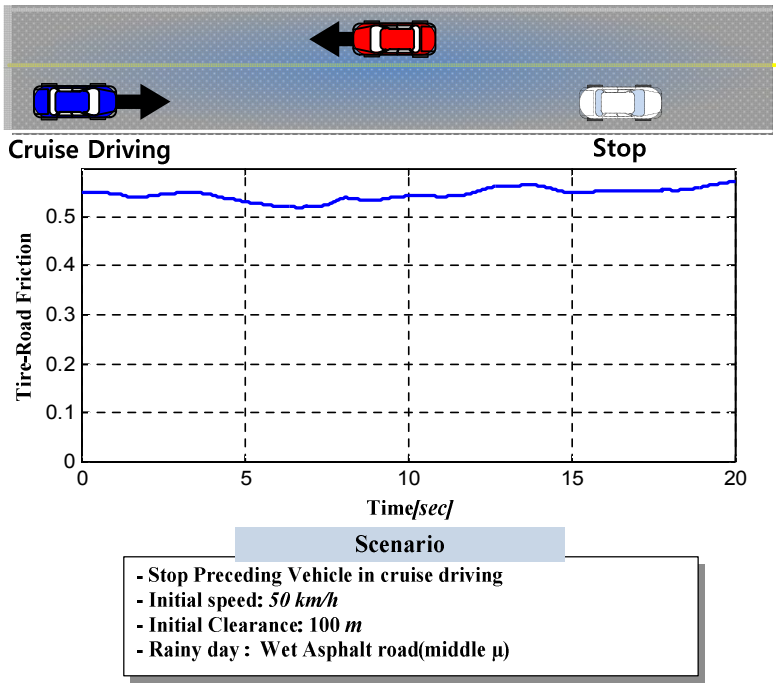

Figure 4.5 Simulation scenario to evaluate the performance of enhanced longitudinal safety: with/without tire-road friction information

As shown in the velocity profile in Figure 4.6, until the vehicle's speed is decreasing by the controller, the longitudinal tire force was not generated and tire-road friction couldn't be estimated. Therefore, as follow the previous chapter, initial tire-road friction was updated as 0.5 by using the rain-sensor signal. After the braking by the controller, the longitudinal tire force are estimated and its values are similar with tire model of the middle mu case. As a result, estimated tire-road friction has little difference with real values.

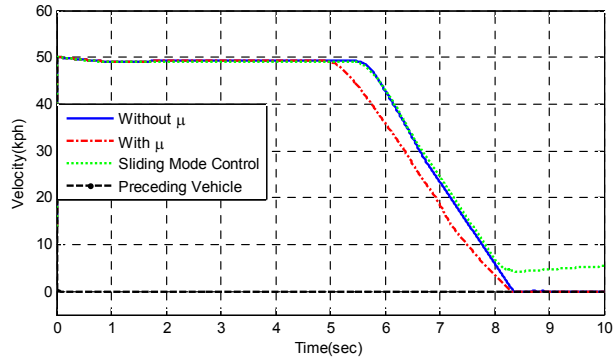

(a) Velocity

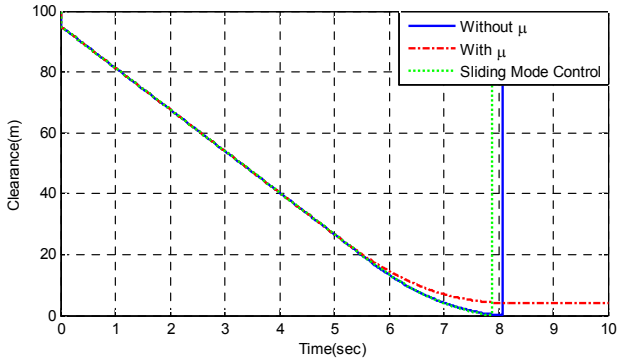

(b) Clearance

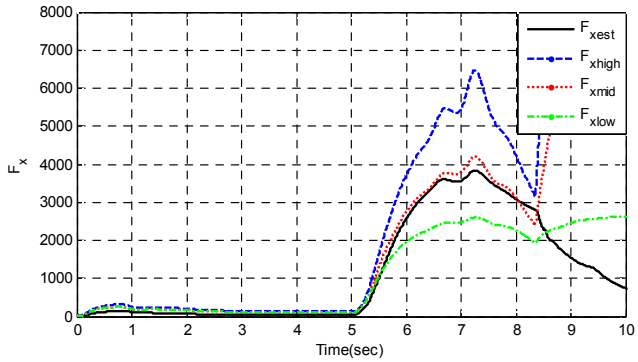

(c) Longitudinal Tire Force

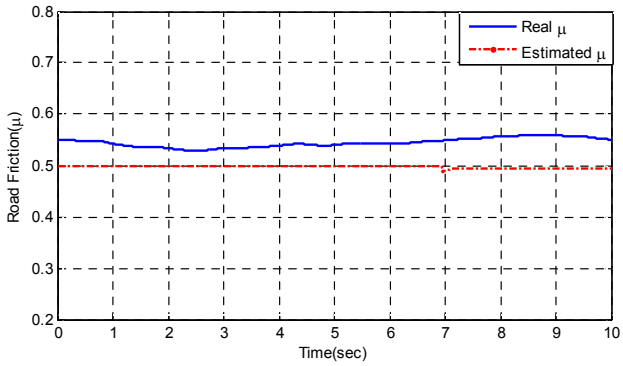

(d) Tire-road friction coefficient

Figure 4.6 Simulation results: with/without tire-road friction information

As decreasing of the clearance and the relative velocity to stop vehicle, safety indices values also decreasing rapidly. As shown in Figure 4.7-(a), because of the maximum acceleration was reduced by the estimated tire-road friction, warning index of the 'with μ' represent as a smaller value than 'without σ' case. TTC values of the both case are calculated as same value, because the definition of the TTC consist of relative velocity and clearance which weren't influenced by the tire-road friction. However, braking related threshold values of the 'With μ' were calculated higher level caused by the increasing braking distance. In contrast, in the case of the 'without μ', threshold values are determined as if given driving situation is in the dry asphalt road. Hence, Control mode decision of the 'With μ'case was changed faster than 'Without σ'case about 0.5s. Also, in the case of 'without μ', because the longitudinal tire force was saturated in partial braking mode by middle tire-road friction, vehicle's acceleration couldn't generate as desired value. Consequentially, rear-end collision could prevent only 'with μ' case. Although, minimum clearance is bigger than dry

asphalt case which was caused by under estimated tire-road friction coefficient, it was effective to prevent rear-end collision in changed tire-road friction condition by the proposed longitudinal safety control algorithm by using the estimated tire-road friction information.

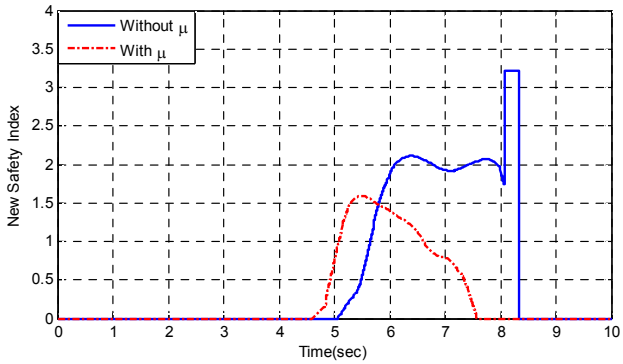

(1) New Safety Index

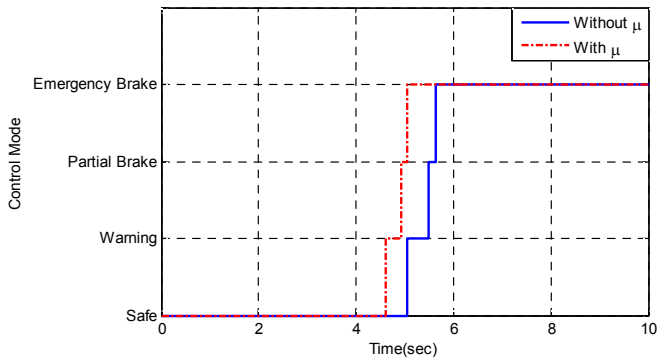

(b) Control Mode

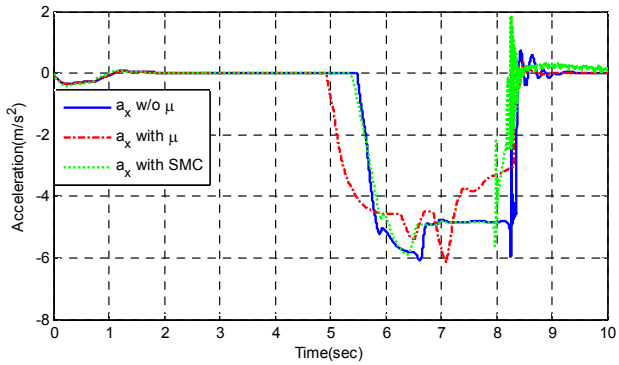

(c) Longitudinal Acceleration

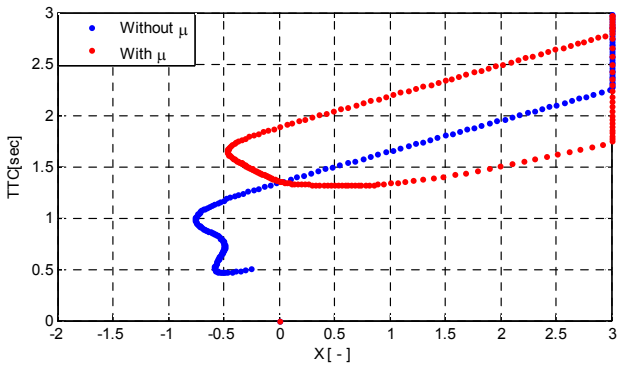

(d) TTC – Warning Index

Figure 4.7 Simulation results: with/without tire-road friction information

To confirm the robustness of the 'With μ' case from the changed tire-road friction, the simulation was conducted 100 iteration in the wet asphalt scenario. As shown in Figure 4.8, in the case of the 'without μ' also could prevent the rear-end collision sometimes. However, it couldn't guarantee the collision avoidance in the most case. On the other hand, 'With μ' case could prevent rear-end collision in all iteration.

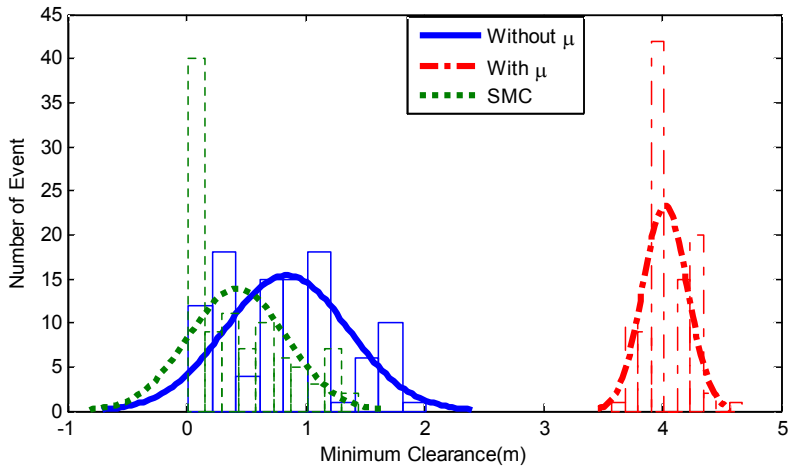

Figure 4.8 Simulation results from 100 iterations:

with/without tire-road friction information

Table 4.2 Results of 100 simulation with/without tire-road friction information

	Without μ	*With μ*	*SMC*
Mean	0.84	4.02	0.43
Variance	0.27	0.04	0.17
Standard Deviation	0.52	0.18	0.41
Number of Crash	13/100	0/100	39/100

Chapter 5

Conclusions

A vehicle longitudinal safety control algorithm for collision avoidance using environment information and a sensor information have been proposed in this dissertation. In order to achieve safe collision avoidance, safety indices based automated braking is determined to prevent rear-end collision.

To develop the new longitudinal safety index, characteristics of existing safety indices were discussed through a theoretical comparison. As a results, a 'Time To Collision' and an 'Warning Index' were used for new longitudinal safety index for driving safety monitoring. Threshold values of safety index were not only determined the physical collision risk but also by the driver's characteristic to achieve 'safe and acceptable' control algorithm. Especially, threshold values were determined based on the physical capability, such as Last Point To Brake(LPTB), Last Point To Steer(LPTS) and analysis results of the manual driving data. By using these safety indices and threshold values, the control mode determines warning level and braking level to maintain the longitudinal safety.

For robust control mode decision, the simple static theory and Kalman filter considering the measurement noise are used in this research. The fusion module

receives detections and, the module tracks from the individual sensors and merges them to a consistent environment description. This includes classification of the observed objects and their dynamics. This is due to the fact that the data is derived from two separate sensors and fused, matched and then approved. In this research, the RADAR sensor and the Vision sensor are used. From the covariance matrix of the Kalman filter and simple definition of the deviation of the function, expected error range of the TTC and the warning index from the measurement noise can be defined. By using the expected error, the threshold of each safety index was determined for safety monitoring of the driving situation.

To estimate the tire-road friction information, friction estimated module which was conducted by Cho in the previous research was used. To make up for unreliability in normal steady driving situation, it is assumed that in the case of normal steady-straight driving condition, the given friction parameters are updated by using the temperature sensor and rain sensor signal. Friction potential affects the maximum predicted accelerations of vehicle longitudinal dynamic. By using the collected obstacle information and tire-road friction information, the TTC of the LPTB, LPTS and the warning index was redefined. As a results, redefined safety indices by using the tire-road friction can detect the collision risk earlier in the non-dry asphalt driving situation.

The proposed vehicle longitudinal safety algorithm was evaluated through computer simulations using vehicle simulation software, CARSIM and MATLAB/Simulink. To classify the enhanced safety performance by the proposed longitudinal safety algorithm, emergency braking in steady following

driving and stop preceding vehicle in the rainy day situation were conducted. Also, to confirm the robustness of the proposed control algorithm, the simulation was conducted 100 iteration in the same scenario. From simulation results, it can be concluded that the proposed longitudinal safety algorithm by using the sensor information analysis and environment information enhance the longitudinal safety and guarantee the robust capacity from the sensor uncertainty and various road condition.

Bibliography

[A. Bose 01] A. Bose and P. Ioannou, Analysis of traffic flow with mixed manual and intelligent cruise control vehicles: theory and experiments, California Path Research Report, UCB-ITS-PRR-2001-13, 2001.

[Ahn 11] Changsun Ahn, Huei Peng, and H. Eric Tseng," Robust Nonlinear Observer To Estimation Road Friction Coefficient and Tire Slip Angle" , 2011 American Control Conference on O'Farrell Street, San Francisco, CA, USA June 29 - July 01, 2011

[An06] X. An, M. Wu, H. He, "A Novel Approach to Provide Lane Departure Warning Using Only One Forward-Looking Camera", Proc. Int. Symp. Collaborative Technologies and Systems, pp.356-362, 2006.

[Aoki11] H. Aoki, Nguyen Van Quy Hung, H. Yasuda, "Perceptual Risk Estimate for Collision Avoidance by Braking and Steering", FAST 2011, Tokyo, Japan, 2011.

[Bakker 87] Bakker, E., Nyborg, L. and Pacejka, H.B.: Tire Modelling for Use in Vehicle Dynamic Studies. SAE Paper No. 870421, 1987.

[Barber, P]Barber, P. et al. "Advanced collision warning systems", IEE Colloquium, Vol. 234, pp. 2/1-2/9.

[B. Song 00] B. Song, D. Delorme and J.Werf, Cognitive and hybrid model of human driver, Proceedings of the IEEE Intelligent Vehicles Symposium 2000, Dearborn (MI), USA, October 3–5, 2000.

[Bundesamt13] Statistisches Bundesamt, Wiesbaden, "Verkehrsunfälle 2012," in Fachserie 8, Reihe 7, 2013.

[Carlson 05] Christopher R. Carlson, J. Christian Gerdes, “Consistent Nonlinear Estimation of Longitudinal Tire Stiffness and Effective Radius”, IEEE Transaction on control system technology, Vol. 13(6) , pp 1010-1020, 2005.

[Cho 10] Wanki Cho, Seungwuk Moon, Sihyoung Lee, and Kyongsu Yi, 2010, "Intelligent Vehicle Safety Control Based on Index plane",AVEC 2010

[Cho 11] Wanki Cho, “Tire Information based Unified Chassis Control for Agility and Vehicle Stability Improvement[Ph.D. thesis]”, Seoul National University, Seoul, Korea, 2006.

[Choi 13] Inseong, Choi, Seongwoo, Cho and Byungdo, Kang,” An Overview on Establishing Safety Assessment Standard of Longitudinal Active Safety System in Korea”, ESV 2013-0490.

[C. Lee 02] C. Lee and K.Yi, An investigation of vehicle-to-vehicle distance control laws using hardware-in-the loop simulation, J. KSME, Part A, 26(7), (2002), pp. 1401–1407.

[D. Delorme 01] D. Delorme and B. Song, Human driver model for smart AHS, California PATH Research Report, UCB-ITS-PRR-2001-12.

[Dugoff 69] Dugoff, Howard, Paul S. Fancher, and Leonard Segel. Tire performance characteristics affecting vehicle response to steering and braking control inputs. No. 105 pp. 1969.

[Ferrara 08] A. Ferrara and C. Vecchio, “Second-order sliding mode control of a platoon of vehicles,” International Journal of Modelling, Identification and Control, vol. 3, no. 3, pp. 277–285, 2008.

[Fancher 00] P. Fancher et al., Human-centered design of an ACC-with-braking and forward-crash-warning system, Proceeding of AVEC2000, 5th

International Symposium on Advanced Vehicle Control, Ann Arbor, Michigan, USA, 2000.

[H. Peng 02] H. Peng, Evaluation of driver assistance systems-A human centered approach, Proceedings of AVEC2002, 6th International Symposium on Advanced Vehicle Control, Japan, 2002.

[James 05] James D. MacIssac Jr & Dr. W. Riley Garrott, "Preliminary Findings of the Effect of Tire Inflation Pressure on the Peak and Slide Coefficients of Friction", NHTSA Technical Report, DOT 809 428, 2005

[Jansson08] J. Jansson and F. Gustafsson, "A framework and automotive application of collision avoidance decision making," Automatica, vol. 44, no. 9, pp. 2347–2351, 2008.

[J. Zhou 04] J. Zhou, and H. Peng, Range policy of adaptive cruise control for improved flow stability and string stability, Proceedings of the 2004 IEEE international Conference on Networking, Sensing and Control, Taipei, Taiwan, March 21–23, 2004.

[Kondo 06] Kondo, T. et al. "Identification of visual cues and quantification of drivers' perception of proximity risk to the lead vehicle in car-following situations", Proc. of DSC Asia/Pacific 2006, 2006, pp. 1-11.

[Kusano11] K. D. Kusano, H. Gabler, "Method for Estimating Time to Collision at Braking in Real-World, Lead Vehicle Stopped Rear-End Crashes for Use in Pre-Crash System Design", SAE 2011

[K. Yi 01] K. Yi et al., A Vehicle Control Algorithm for Stop-and-Go Cruise Control, J. Autom. Eng. Proc. Inst. Mech. Eng. 215 (2001), pp. 1099–1115.

[K.Yi 01] K.Yi andY.Kwon,Vehicle-to-vcehicle distance and speed control using an electronic vacuum booster, JSAE Review 22, (2001), pp. 403–412.

[K.Yi 02] K.Yi et al., Implementation and vehicle tests of a vehicle stop-and-go cruise control system, J. Automo. Eng. Proc. Inst. Mech. Eng. Part D, 216 (2002), pp. 537–544.

[Larson 05] Larson, R., Fowler, G.F., “Driver Crash Avoidance Behavior: Analysis of Experiment Data Collected in NHTSA’s Vehicle Antilock Brake System (ABS) Research Program, ASE Technical Papers 2005-01-0423

[Lee 11] Taeyoung Lee, Kyongsu Yi and Changhyun Jeong, “Integrated Stochastic Driver Model for Evaluation of the Vehicle Active Safety Systems”, First International Symposium on Future Active Safety Technology toward zero-traffic-accident September 5-9,2011, Tokyo, JAPAN

[Lee 11] Taeyoung Lee, Beomjun Kim, Kyongsu Yi and Changhyun Jeong,“ Development of Lane Change Driver Model for Closed-loop simulation of the Active Safety System”, 14th IEEE International Intelligent Transportation Systems Conference (ITSC), The George Washington University (GWU) at Washington, DC, October 5-7, 2011

[Lie 14] Guo Lie, et all. ,“Advanced Emergency Braking Controller Design for Pedestrian Protection Oriented Automotive Collision Avoidance System”,The Scientific World Journal 2014

[M. Bando 95] M. Bando et al., Dynamic model of traffic congestion and numerical simulation, Phy. Rev. E51, pp. 1035–1042, 1995.

[Minoiu09] N. Minoiu,. M. Netto, S. Mammar, B. Lusetti,.”Driver Steering Assistance for Lane Departure Avoidance” Control Engineering Practice, Vol. 17, pp. 642–651, 2009

[Moon08] S. Moon, K. Yi, “Human driving data-based design of a vehicle adaptive cruise control algorithm”, Vehicle System Dynamics, Vol. 8, No. 4, pp.

111-123, 2008.

[Moon09] S. Moon, I. Moon, and K. Yi, “Design, tuning, and evaluation of a full-range adaptive cruise control system with collision avoidance”, Control Engineering Practice, Vol. 17, No. 4, pp.442-455, 2009.

[Nouveli`ere 07] L. Nouveli`ere and S. Mammar, “Experimental vehicle longitudinal control using a second order sliding mode technique,” Control Engineering Practice, vol. 15, no. 8, pp. 943–954, 2007.

[Pipes 53] L.A. Pipes, An operation analysis of traffic dynamics, J. Appl. Phys., 24 (1953), pp. 271–181.

[R. Holve 95] R. Holve et al., Adaptive fuzzy control for driver assistance in car-following, Proceedings of the 3rd European Congress on Intelligent Techniques and Soft Computing-EUFIT’95,Aachen, Germany, pp. 1149–1153,August 1995.

[Rimini05] M. Rimini-Doering, T. Altmueller, “Effect of Lane Departure Warning on Drowsy Drivers’ Performance and State in a Simulator”, PROCEEDINGS of the Third International Driving Symposium on Human Factors in Driver Assessment, Training & Vehicle Design, pp. 88-95, 2005.

[Road Traffic Accidents in Korea 2009] “Road Traffic Accidents in Korea 2009”, Traffic Accident Analysis Center, Road Traffic Authority, Korea.

[Road Traffic Accidents in Korea 2012] Road Traffic Accidents in Korea 2012, Published by Traffic Accident Analysis Center Korea Road Traffic Authority, Korea

[R. Schram 13] Richard Schram, Aled Williams and Michiel van Ratingen, “Implementation of Autonomous Emergency Braking (AEB), The next step in EURO NCAP’s safety assessment”,ESV 2013-0269

[Seiler98] P. Seiler, B. Song, and J. K. Hedrick, “Development of a Collision Avoidance System”, Proc. SAE Conference, pp. 97-103, 1998.

[T. Miyazaki 01] T. Miyazaki et al., Modeling of human behaviors in real driving situations, 2001 IEEE Intelligent Transportation Systems Conference Proceedings, pp. 645–648, Oakland (CA), USA, August 25–29, 2001.

[Vahidi03] A. Vahidi, and A. Eskandarian, “Research Advances in Intelligent Collision Avoidance and Adaptive Cruise Control”, IEEE Transactions on Intelligent Transportation Systems, Vol. 4, No. 3, pp.143-153, 2003.

[Yeo11] H. Yeo, A. Skabardonis, “Microscopic Fundamental Relationships between Vehicle Speed and Spacing in View of Asymmetric Traffic Theory”, Intelligent Transportation Systems (ITSC) , pp. 1410-1414, 2011

[Yamazaki 97] S. YAMAZAKI, O. FURUKAWA, and T. SUZUKI, “Study on Real Time Estimation of Tire to Road Friction”, Vehicle System Dynamics Supplement 27 (1997), pp. 225-233

[Yi 02] Jingang Yi, “Adaptive Emergency Braking Control With Underestimation of Friction Coefficient”, IEEE TRANSACTIONS ON CONTROL SYSTEMS TECHNOLOGY, VOL. 10, NO. 3, MAY 2002,

[Zhang 04] Zhang, J. and Ioannou, P., Control of heavy-duty trucks: environmental and fuel economy considerations, California PATH Program, Inst. Transp. Studies, Univ. California, Berkeley, California PATH Research Rep. UCB-ITS-PRR-2004-15, 2004

[Zhang 06] Z. Zhang, Automatic guidance system based on DGPS for rice transplanter [Ph.D. thesis], South ChinaAgriculturalUniversity, Guangzhou, China, 2006.

[Zhu 12] Y. Zhu and M. Y. Feng, “Research on intelligent vehicle autonomous

overtaking based on single neuron PID control,” in Proceedings of the International Conference on Cloud Computing and Intelligent Systems, pp. 1192−1195, Hangzhou, China, 2012.

초 록

타이어 노면 마찰 추정 및 센서 불확실성을 활용한 강건한 자동비상제동알고리즘 개발

현대사회의 자동차 관련 기술의 발전과 더불어, 네비게이션 시스템이나 DMB, 등의 운전자 편의 장비들의 보급이 활발히 이루어 졌지만, 이러한 편의장치의 확대로 인하여 운전자의 운전에 대한 집중력의 하락으로 인한 사고 위험이 증가하여, 이와 관련된 사고의 발생 빈도가 증가하는 추세이다. 이러한 추세에 따라, 차량의 안전시스템에 대한 필요성과 인식이 확대되어, 전방차량과의 충돌을 방지하고, 전방 충돌이 발생하는 경우 충격을 완화시켜 줄 수 있는 충돌 충격 완화시스템(CDM: Collision Damage Mitigation), 전방충돌 경보시스템(FCW: Forward Collision Warning)등의 시스템이 활발히 연구되고 있으며, 특히 자동비상제동장치(AEBS: Advanced Emergency Braking System)의 경우, 국제 표준화 기구(ISO: International Organization for Standardization)를 통하여 시스템의 의무장착을 위한 법령이 추진되는 추세이다. 이러한 추세에 맞춰, 다양한 종방향 안전 시스템이 개발되어 왔으며, 양산 차량에 장착되고 있다.

하지만, 이러한 안전 시스템은 운전자에게 직접적인 경보신호를 제공하고, 차량에 직접적인 제동을 인가하기 때문에 운전자가 위험하다고 판단하지 않는 시점에 경보 또는 제동을 수행하게

된다면 운전자의 불편함과 이질감을 상승시키게 된다. 따라서 차량의 종방향 안전성을 보장하며, 운전자의 거부감이 들지 않는 종방향 안전 시스템을 구성하기 위하여, 운전자의 주행특성과 물리적 충돌위험에 기반한 자동비상제동알고리즘을 구성하였다.

또한, 감지센서에서 발생하는 오차 및 외란의 영향으로 인하여 의도하지 않은 성능 저하를 야기 할 수 있으며, 제동이 수행되는 과정에서 도로의 상태에 따라 제동성능이 크게 영향을 받게 되므로, 도로의 노면상태와 연관성을 고려하여 차량의 제어 성능을 보다 향상 시킬 수 있는 종방향 안전 시스템의 개발이 필요하다. 따라서 본 논문에서는 도로 정보 및 센서정보의 분석을 기반으로 한 종방향 차량 안전성 제어에 대한 내용을 다룬다.

도로의 특성의 경우, 기존의 연구결과를 바탕으로 종/횡방향 차량거동 및 환경에 따라 도로의 노면마찰을 추정할 수 있는 노면마찰추정모듈을 활용하였다. 이러한 분석을 기반으로 하여, 종방향 안전 제어 시스템에서는 전방 차량의 정보와 자차량 정보 및 도로의 노면정보를 이용하여 현재의 주행상태에 대한 위험도 모니터링을 수행한다. 위험도 모니터링을 통하여 차량의 상태가 위험한 상태로 진입하게 되면, 주행상태와 도로 상태를 고려하여 제어 입력을 계산하여, 차량의 종방향 안전도를 향상시키기 위한 제어를 수행한다. 센서정보의 경우, 실제 양산에 활용되는 2종의 센서를 활용하여, 실차 실험을 통한 센서 측정 데이터를 수집하여 측정과정에서 발생할 수 있는 센서 특성을 분석을 수행하였으며, 분석된 센서의 특성을 활용하여 제어에 필요한 측정값을 보정하여 보다 정확하고 신뢰도 있는 제어가 수행될 수 있도록 하였다.

구성된 자동비상제동시스템의 성능을 확인하기 위하여, CarSim 차량동역학 시뮬레이션 프로그램을 이용하였으며, 시뮬레이션을 통하여 종방향 안전 제어 시스템을 통한 '전방충돌 위험상황'에서의 안전성 확보 성능을 검증하였다. 이러한 결과를 통하여 본 논문에서 제안한 종방향 안전 제어 시스템을 통하여 다양한 도로상황과 센서정보의 오차상황에 대하여 종방향 충돌을 방지할 수 있는 제어를 수행할 수 있으며, 이를 통하여 차량의 종방향 안전도를 향상시킬 수 있음을 확인할 수 있다.

주요어: 자동비상제동장치, 센서 오차, 타이어-노면 마찰계수 추정, 종방향 차량 안정성, 충돌회피

학 번: 2007-22993